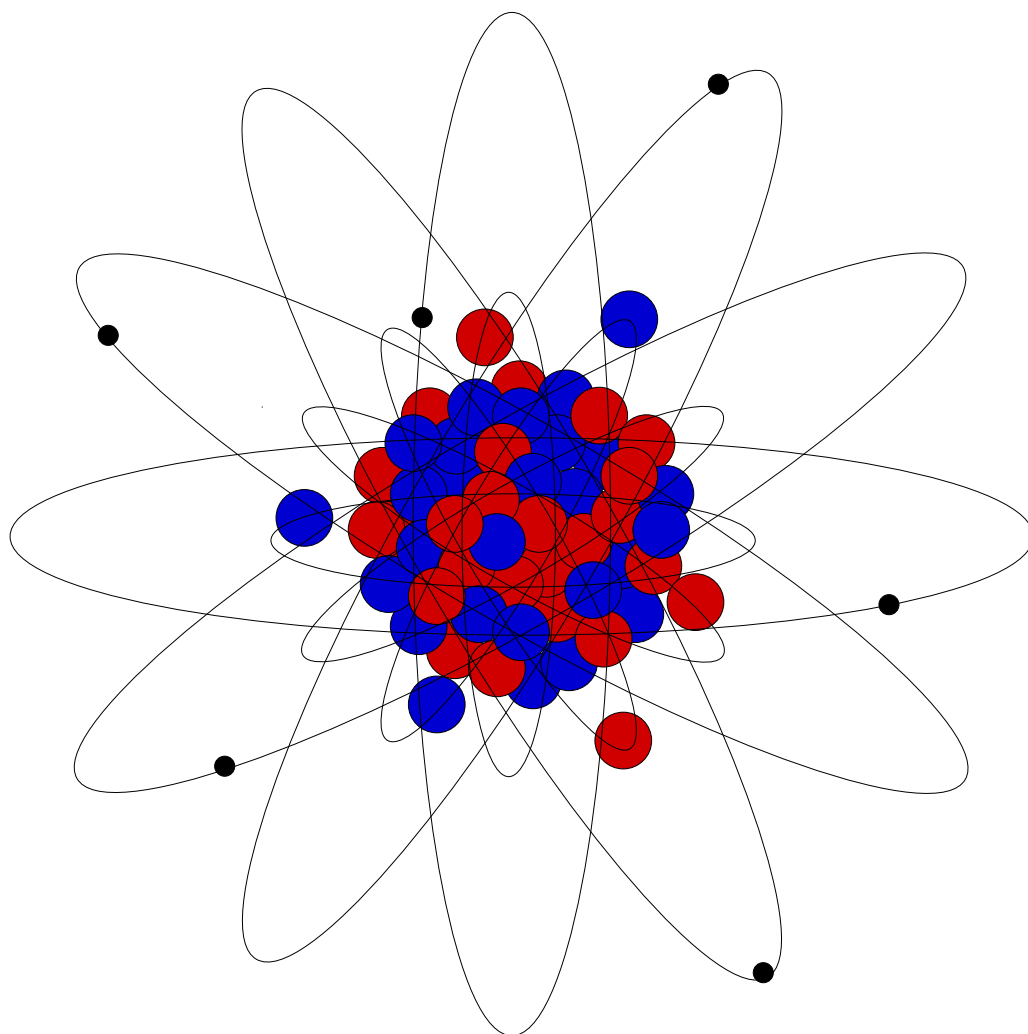


# In Quest of Excited States in $^{61}\text{Ga}$

Lise-Lotte Andersson

Master Thesis



Department of Physics  
Division of Nuclear Physics  
Lund University  
2004  
LUNFD6/(NFFR-5022)1-47/(2004)



**LUND**  
UNIVERSITY

## Abstract:

In an attempt to extend the knowledge of mirror nuclei into the mass  $A = 60$  region, the fusion evaporation reaction  $^{40}\text{Ca} + ^{24}\text{Mg}$  at 104 MeV was used to identify excited states in the hitherto unknown isotope  $^{61}_{31}\text{Ga}_{30}$ .

The experiment took place in August 2003 at the Holifield Radioactive Ion Beam Facility at Oak Ridge National Laboratory (ORNL), Tennessee. The experimental set-up comprised the Ge array CLARION, the Recoil Mass Spectrometer, and an Ionisation Chamber. The collaboration saw students and physicists from Lund University, Sweden, Keele University, UK, and the Physics Division at the ORNL.

During the analysis elaborate Doppler correction routines using both the segmentation of the CLARION Ge detectors and the total energy deposited in the ion chamber have been developed along with novel approaches to obtain optimal  $Z$ -resolution by comparing several combinations of the three energy-loss signals in the ion chamber, so called energy loss functions.

Transitions in  $^{61}\text{Ga}$  are clearly identified for the first time. The strongest transition at 271 keV is believed to be the “mirror” transition to the 124 keV  $5/2^- \rightarrow 3/2^-$  groundstate transition in  $^{61}\text{Zn}$ . The rather large energy difference of 150 keV is most likely due to Coulomb monopole contributions such as radial or the electromagnetic spin orbit interactions. The former may play a significant role as  $^{61}\text{Ga}$  is bound only with 200 keV. The latter arises from proton vs. neutron excitations from the  $p_{3/2}$  into the  $f_{5/2}$  orbital. Large scale shell-model calculations seem to support the preliminary interpretation.

# Contents

<b>Introduction</b>	<b>2</b>
<b>1 The Experiment</b>	<b>5</b>
1.1 Experimental Methods . . . . .	5
1.2 CLARION . . . . .	7
1.3 Recoil Mass Spectrometer . . . . .	8
1.3.1 $A/Q$ . . . . .	8
1.3.2 Efficiency . . . . .	10
1.3.3 Charge-Reset Foil . . . . .	10
1.4 The Detectors . . . . .	12
1.4.1 The Micro Channel Plate . . . . .	12
1.4.2 The Ionisation Chamber . . . . .	12
<b>2 Data Handling</b>	<b>15</b>
2.1 Data Sorting . . . . .	15
2.2 Calibration and Alignment of the Ge-Detectors . . . . .	16
2.3 Calibration of the Ionisation Chamber . . . . .	16
2.4 Optimising the $Z$ Separation . . . . .	20
<b>3 Data Analysis and Results</b>	<b>21</b>
3.1 The Recoil- $\gamma$ Matrix . . . . .	21
3.1.1 The IC Spectrum . . . . .	21
3.1.2 The $\gamma$ -Ray Spectrum . . . . .	22
3.2 Transitions in $^{61}\text{Ga}$ . . . . .	27
3.2.1 Improving the $^{61}\text{Ga}$ Gate . . . . .	27
3.2.2 Finding Transitions . . . . .	27
3.2.3 Confirmation via IC Spectra . . . . .	30
3.2.4 Recoil- $\gamma\gamma$ Analysis . . . . .	30
3.2.5 The Decay Scheme . . . . .	31
3.3 Relative Cross-Sections . . . . .	35
<b>4 Comparing Theory and Experiment</b>	<b>37</b>
4.1 Mirror Energy Difference . . . . .	40
<b>5 Conclusion and Outlook</b>	<b>43</b>
<b>Acknowledgements</b>	<b>44</b>
<b>References</b>	<b>47</b>



# Introduction

The aim of this Master thesis is to find and identify the low-lying energy levels in  ${}^{61}_{31}\text{Ga}_{30}$  nuclei and compare the structure of the  ${}^{61}\text{Ga}$  nucleus with its mirror nucleus  ${}^{61}_{30}\text{Zn}_{31}$ . Mirror nuclei have the same mass but their proton and neutron numbers are interchanged. Since the nuclear force is thought to be charge independent their structure is expected to be more or less identical. Small differences in structure may, however, be explained via the effect of the Coulomb force.

The Experimental Nuclear Structure Group in Lund is particularly interested in studying mirror nuclei and the differences between them. Since mirror nuclei in theory are supposed to be almost identical in structure one may be surprised to find several discrepancies between them. The differences may, however, contribute to a wider and more profound understanding of interactions inside the nucleus and the parameters involved in creating the intrinsic structure and properties of a particular nucleus.

The experiment analysed in this Master thesis was performed at the Oak Ridge National Laboratory (ORNL), Tennessee, more specifically at the Holifield Radioactive Ion Beam Facility (HRIBF). A  ${}^{40}\text{Ca}$  ion beam of 104 MeV was projected on a thin  ${}^{24}\text{Mg}$  target foil and via a fusion-evaporation reaction a number of nuclei were produced. The main purpose of the experiment was to produce  ${}^{62}\text{Ge}$  nuclei. The nuclear structure of this isotope has not been mapped earlier as its production cross section is very small.

The estimated total run time of the experiment was seven days. The estimation was built on the time required to produce enough  ${}^{62}\text{Ge}$  nuclei to study the first few excited states in that nucleus. The experiment was granted three days of preparatory beam time, referred to as week one, and 5 days (110 h) of beam time for the running of the experiment in a steady-state mode, referred to as week two. Due to the fact that the ion source, required to produce the  ${}^{40}\text{Ca}$  beam, broke down twice during the running of this experiment only about 55 h of total run time, excluding the preparatory beam time, was obtained in the end. Complications with the intensity of the ion beam also occurred, which further decreased the probability of producing a sufficient amount of  ${}^{62}\text{Ge}$ , and hence also  ${}^{61}\text{Ga}$ , nuclei.

The data sorting and analysis of the experiment are described in this thesis. I have tried to keep the different steps in chronological order. The first chapter aims to give a basic understanding of the experimental equipment, especially of the Recoil Mass Spectrometer (RMS) and the Ionisation Chamber (IC) used to detect the produced nuclei. The second chapter gives some details about the preparatory work, and chapter three contains the methods of analysing data, the identified transitions are also presented and discussed there. Chapter four gives an comparison of theory

and experimental results and chapter five concludes the results and provides an outlook for further investigations of the  $^{61}\text{Ga}$  nucleus.

The calibrations and preparation of data performed for the analysis in this Master thesis were performed in cooperation with Emma Johansson, and so it is inevitable not to refer to her thesis [1]. We have, however, investigated the excited states in different nuclei and our reports aim to explain different parts of the experimental equipment and the preparatory data handling.

# Chapter 1

## The Experiment

The aim of this chapter is to give an overlook of the experiment and a basic understanding of the experimental setup. The RMS and surrounding equipment such as the Ion Chamber are explained fairly detailed in this report, whereas CLARION and the Ge-detectors are mentioned more briefly. Further information can be found in Emma Johansson's Master thesis [1].

### 1.1 Experimental Methods

In the experiment the  $^{61}\text{Ga}$  nuclei are produced via a fusion-evaporation reaction, illustrated in Fig. 1.1. An incidenting beam nucleus hits the target and forms, via fusion, a compound nucleus. This compound rotates quickly and is highly excited, i.e., it is very unstable and has a short lifetime. By emitting particles such as neutrons, protons, and  $\alpha$ -particles the compound will lose some of its energy. The particles, which carry both kinetic energy, binding energy, and angular momentum are said to be evaporated. Which particles are emitted depends only on the energy of the system; it decays according to the statistical probabilities of different reaction channels. The more energy the system contains the more particles are likely to be evaporated and each reaction channel has a cross-section with roughly Gaussian-like shape if plotted as a function of the beam energy. However, in time it will not be energetically possible for the compound nucleus to evaporate more particles and the system will lose its remaining energy by emitting statistical and discrete  $\gamma$ -rays. The discrete  $\gamma$ -rays hold information about the nuclear structure as the energy of them will correspond to the energy difference between the excited levels inside the nucleus. Hence, by detecting these  $\gamma$ -rays, one may map the nuclear energy levels.

In this experiment a  $^{40}\text{Ca}$  beam and a  $^{24}\text{Mg}$  target were used, forming the compound nucleus  $^{64}\text{Ge}$ . By evaporating one proton and two neutrons the, for this Master thesis interesting,  $^{61}\text{Ga}$  nucleus is produced. (See Fig. 1.2)

The cross-sections for different reaction channels may be simulated via an advanced computer program. Some channels of interest for this experiment are shown in Fig. 1.3. By looking at the figure it is possible to see that the cross-section for the 2pn channel has its maximum placed at a slightly higher beam energy than the 3p channel. This is due to the fact that the reaction products are proton rich and need more excitation energy to evaporate a neutron than a proton. The main purpose of the experiment was the identification of excited states in  $^{62}\text{Ge}$ . To produce  $^{62}\text{Ge}$ ,

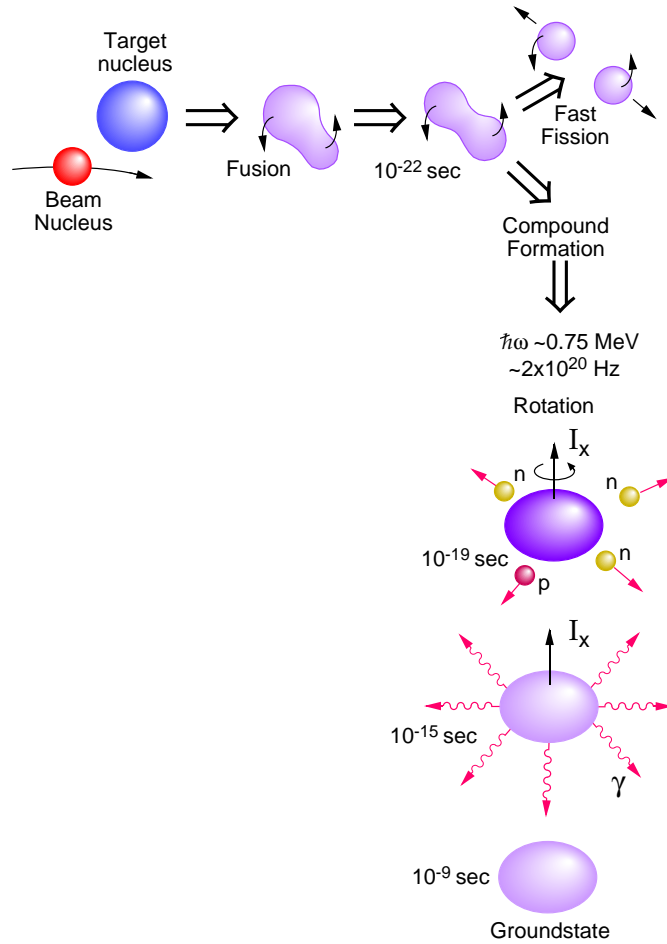


Figure 1.1: The life cycle of a compound nucleus. As can be seen there is a certain probability for the fused particles to undergo fission instead of forming a compound.

which is the  $2n$  reaction channel, the largest cross-section should appear somewhere about 108 MeV. Since the cross-sections for all the other reaction channels increase rapidly in this region a slightly lower beam energy of 104 MeV was chosen for this experiment. A lower beam energy opens fewer reaction channels, which is good in general but is especially important when one wants to identify nuclei with small cross-sections such as  $^{61}\text{Ga}$  and  $^{62}\text{Ge}$ .

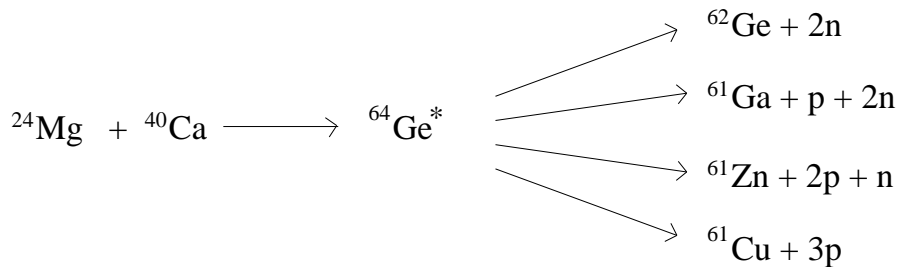


Figure 1.2: The reaction channels of interest from the  $^{64}\text{Ge}^*$  compound nucleus.

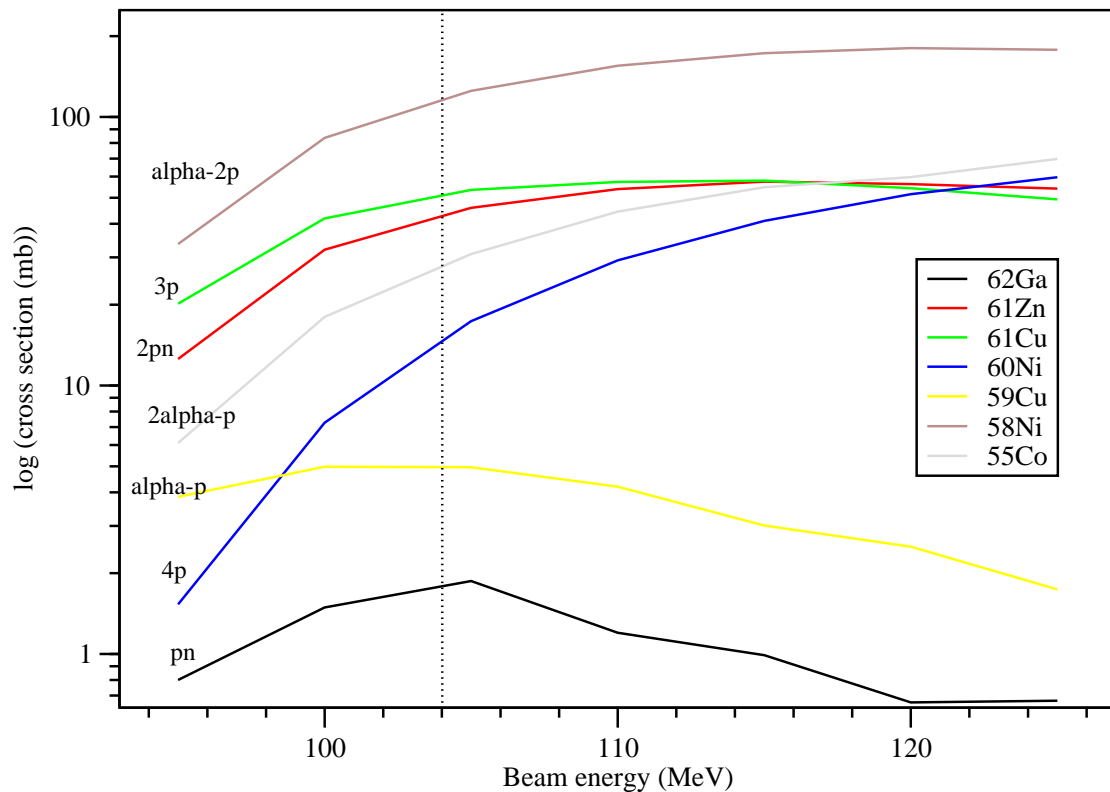


Figure 1.3: The cross-section for different reaction channels. The dotted line indicates the beam energy that was chosen for this experiment.

## 1.2 CLARION

The central piece of the experimental setup is CLARION, the CLOver Array for Radioactive ION beams, which is an array of Ge crystals that detect the  $\gamma$ -rays emitted from the excited nuclei at the target position.

The crystals are combined together four by four into so called clover Ge detectors. There are eleven clover detectors altogether and they are placed in a “ $3\pi$ ” geometry forming the CLARION sphere, a photograph of which is shown in Fig. 1.4. The eleven clover detectors can be divided into three rings placed at  $90^\circ$ ,  $132^\circ$  and  $155^\circ$  with respect to the beam axis, i.e. mainly in the back hemisphere. This placing is rather strategic because the facility often uses a radioactive beam, which scatters and accumulates at forward angles and gives rise to large background radiation. The placement is also advantageous as it keeps the crystals out of the magnetic fields from the Recoil Mass Spectrometer (RMS) which is placed in close connection to CLARION.

Ten of the eleven clover detectors are divided into three sections, so called side channels, to increase the accuracy of determining the incident angle of the  $\gamma$ -rays. This is necessary in order to make high accuracy Doppler corrections and helps when making an add-back correction. More details about these corrections are presented in Sec. 2.2. The total efficiency of the eleven clover detectors has been measured to be 2.2% at 1.33 MeV [2].

For further information about CLARION’s construction and function the reader is recommended to read Emma Johansson’s Master thesis [1].

## 1.3 Recoil Mass Spectrometer

The Ge-detector array is, as mentioned earlier, placed in connection to a RMS, which makes it possible to correlate prompt  $\gamma$ -radiation emitted inside CLARION with the recoils, i.e., the reaction products, detected in the Ionisation Chamber situated at the final focal plane of the RMS. The RMS at HRIBF is a combination of a momentum separator and a mass separator, which allows for an efficient rejection of the primary beam and good transport and identification of the recoils. A schematic picture of the RMS is shown in Fig. 1.4. One sees the two electrostatic dipoles (E), the three magnetic dipoles (D), the seven quadrupoles (Q) and the two sextupoles (S) that form the RMS. Figure 1.4 also indicates the position of three foci; the momentum dispersed focal plane, the achromatic focal plane, and the  $A/Q$  dispersed focal plane.

From the target inside CLARION the products from the fusion-evaporation reactions and primary beam move 75 cm before entering the RMS via the first quadrupole. The ions then travel through the RMS and are finally deposited in the Ionisation Chamber (IC) at the end of the 25 m long flight path.

The first part of the RMS separates the nuclei in momentum,  $P/Q$ , which makes it possible to reject the beam at the momentum dispersed focus, due to the fact that the charge states of the primary beam and the recoils remains fixed for a certain event (see Sec. 1.3.3). After passing through the momentum dispersed focal plane the ions are focused at the achromatic focal plane. The ions may now enter the second part of the RMS, which consists of a mass separator that is used to separate ions by their mass-to-charge ratio independent of their energy. This results in an  $A/Q$  dispersed image at the last focal plane.

The focusing properties of the RMS can be changed by adjusting parameters, so called knobs, to fit various experiments. The knobs are, however, just virtual and consist of a computerised control panel in which parameters such as field strengths in the different components of the RMS may be changed. These adjustments are very important in order to, for example, optimise the  $A$  and  $Z$ -resolution, which is of great importance in this experiment.

Furthermore the RMS can be run in two different modes, diverging and converging. Here the converging mode is chosen, which means that 80 cm after the  $A/Q$  dispersed focus the different masses would converge into a single blob. In diverging mass mode the RMS is designed with an energy acceptance of approximately  $\pm 10\%$  and an  $A/Q$  acceptance of  $\pm 4.9\%$  [5]. The values are compatible for the converging mode.

### 1.3.1 $A/Q$

When running the experiment we know, due to the chosen beam energy, that the recoils will not be fully stripped from their electrons. There is a certain probability of stripping electrons from an atom which makes it useful to introduce a parameter called charge state. The charge state, denoted  $Q$ , refers to the number of stripped electrons, i.e., the number of protons in the nucleus minus the number of electrons that still cling to the atom. Before running an experiment it is possible to calculate the probabilities for a certain atom to enter different charge states. For this experiment calculations were obviously made for  $^{61}\text{Ga}$  and  $^{62}\text{Ge}$  and the probability peaks

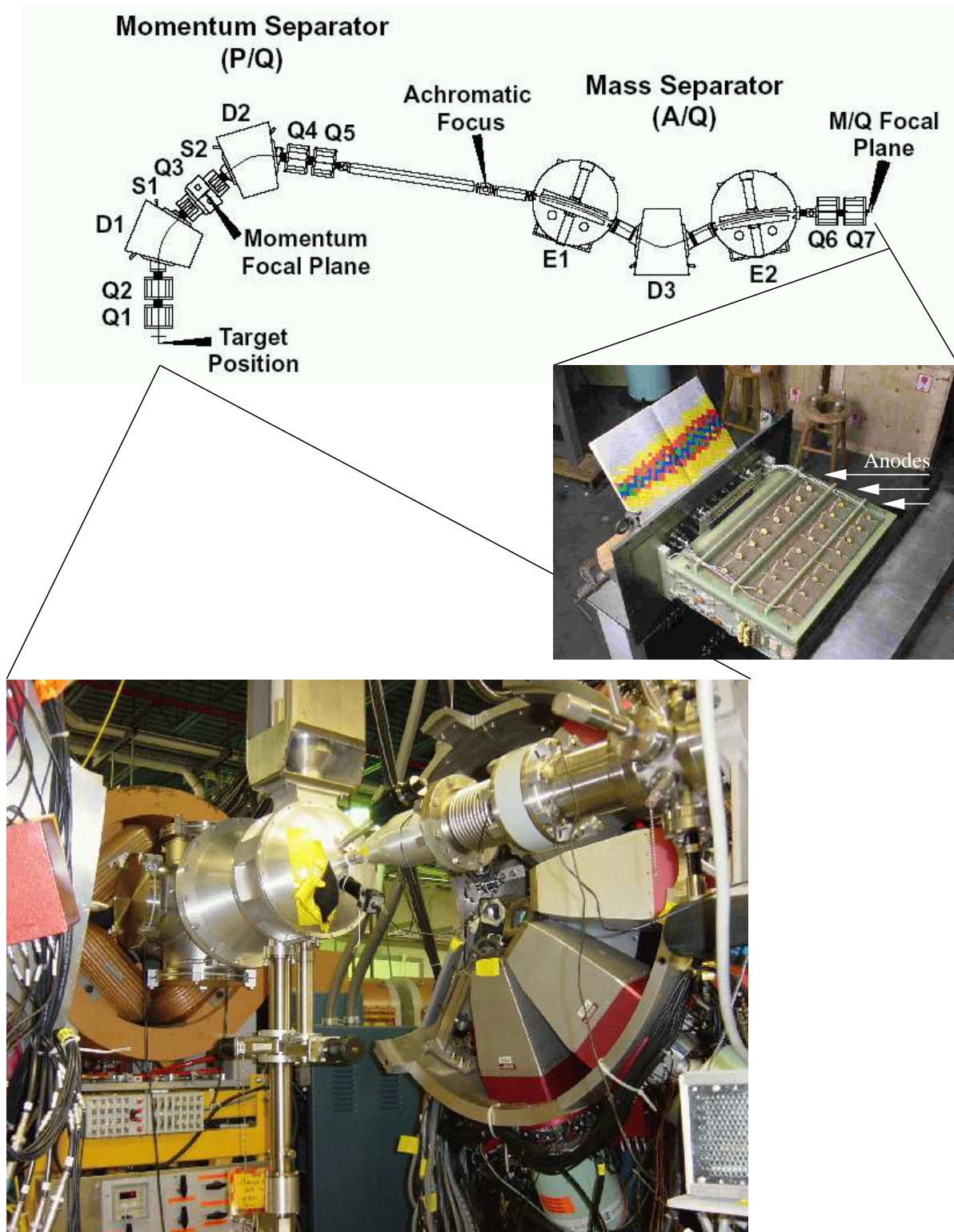


Figure 1.4: (Top) A schematic drawing of the RMS with all its components. The first part is the momentum separator and the second part, which starts after the achromatic focus, is the mass separator [3]. (Middle) A photo of the IC with the three segments of the anode marked out. The recoils enter the IC from the bottom right [4]. (Bottom) A photo of CLARION when it is open. One sees the Ge detectors placed on a sphere surrounding the target chamber. The beam incidents from the right. When running the experiment the two hemispheres are moved together to close the sphere.

were placed at  $Q=18$  and  $19$ . Fig. 1.5 shows how the detected recoils with different  $A/Q$  values will be placed in relation to each other in the focal plane. The vertical lines in the plot indicate the expected upper and lower level of acceptance ( $\pm 4.9\%$  in  $A/Q$  value) if the RMS is optimised at the “ $A/Q$  middle” value. There are, however, just recoils with three different  $A/Q$  ratios, i.e. with three different masses, detected in the left side of the IC, which indicates that due to settings of the RMS a lower  $A/Q$  acceptance, about  $\pm 3.6\%$ , is obtained in this experiment. The three masses can be identified by being investigated separately. It is possible to pick them out one by one and generate  $\gamma$ -ray spectra with intensity versus  $\gamma$ -ray energy. The masses may be determined by finding well known, strong transitions from different nuclei in the three spectra. Hence the plot in Fig. 1.5 will make it possible to optimise the settings of the RMS to receive recoils with the proper mass-to-charge ratio in the IC. In this experiment the RMS was tuned to accept recoils of  $A = 62$  with  $Q = 18.10$  and recoil  $E = 58.2$  MeV.

### 1.3.2 Efficiency

The efficiency of the recoil mass spectrometer is dependent on many intrinsic parameters such as design and construction but it is also dependent on external parameters such as the reaction kinematics and target thickness. It is hence important to use the target, beam, and reaction channels (i.e., beam energy) compatible with the best possible performance to optimise the transmission and mass resolution.

In this experiment a  $^{24}\text{Mg}$  target of thickness  $300 \mu\text{g}/\text{cm}^2$  was used. If the thickness were to be increased, complications such as multiple scattering inside the target would appear with the risk of either scattering the recoils in angles that does not allow them to enter the RMS or to produce an energy distribution in the reaction products that does not allow them to be transmitted through the RMS.

It would also be possible to use a  $^{40}\text{Ca}$  target and a  $^{24}\text{Mg}$  beam instead to get different reaction kinematics. One of the drawbacks of this reaction is that a  $^{40}\text{Ca}$  target very easily oxidises, which may lead to contamination reactions on  $^{16}\text{O}$  in which additional recoils would be produced. Another drawback is that this reaction will give unfavourable kinematics, which will lead to the scattering of recoils inside the target chamber. This would result in fewer recoils entering the RMS. However, the choice of having a  $^{40}\text{Ca}$  beam is not problem free either as the beam is hard to produce, especially at high intensities.

### 1.3.3 Charge-Reset Foil

A charge-reset foil, placed 10 cm downstream from the target, was used in the experimental setup. It prevents the reaction products from losing their charge state. If the recoiling ions have isomers, which may decay through *internal conversion*<sup>1</sup>, they might lose their equilibrium charge state distribution. To prevent this one can use a charge-reset foil, typically consisting of  $20 \mu\text{g}/\text{cm}^2$  carbon. The reset foil gives the ions a new equilibrium charge state distribution before entering the RMS.

---

<sup>1</sup>The nucleus does not decay from its excited state by emitting a photon. Instead the nucleus interacts with the surrounding electrons, which causes one of them to be emitted from the atom.

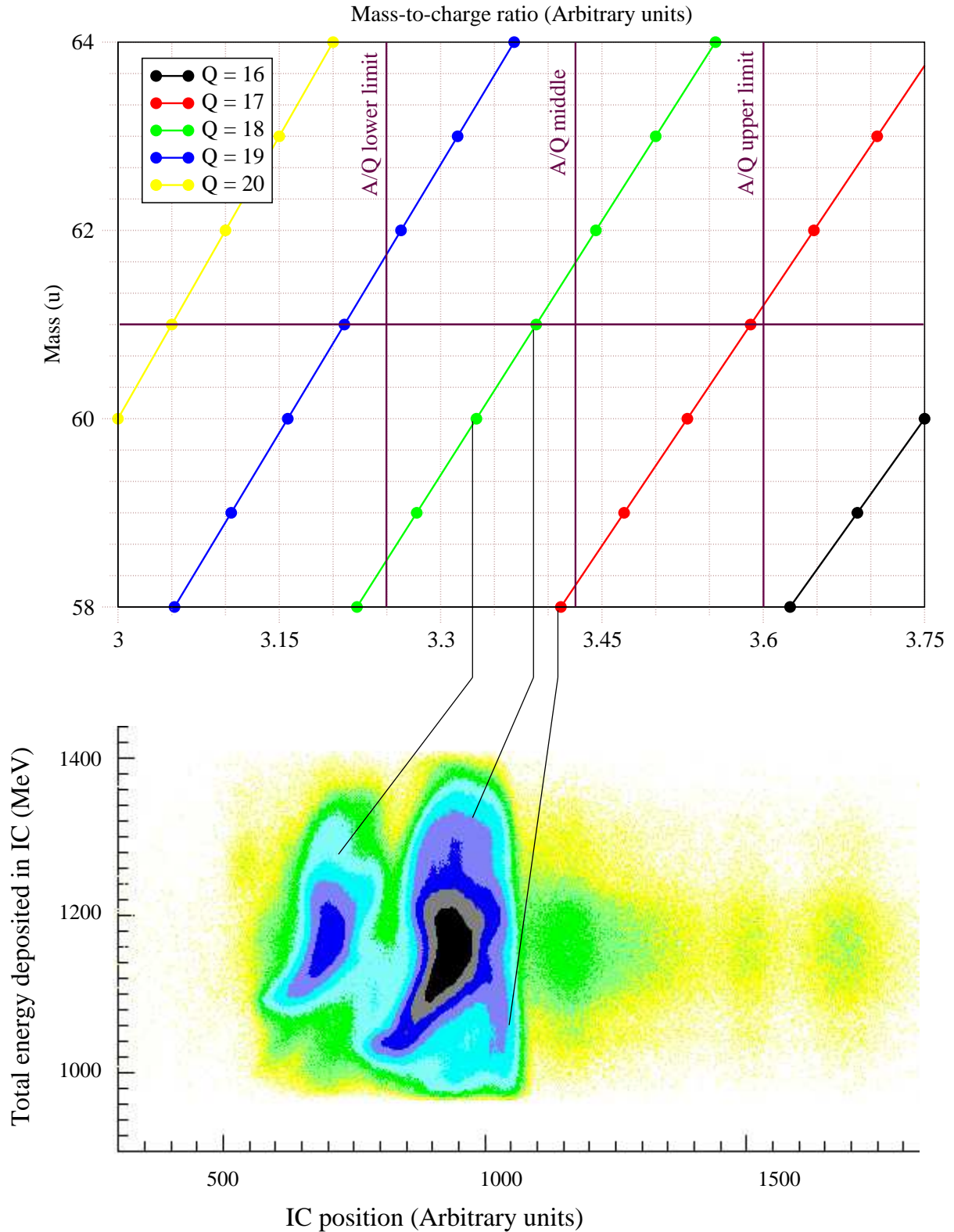


Figure 1.5: (Top) The mass of a recoil plotted against  $A/Q$ . By projecting the dots down onto the  $x$ -axis one may see the predicted position of recoils detected in the IC. (Bottom) The detected recoils in the  $A/Q$  dispersed focal plane. Only the recoils detected in the left side of the IC are shown.

## 1.4 The Detectors

### 1.4.1 The Micro Channel Plate

Earlier a Position Sensitive Avalanche Counter (PSAC) was used to determine the different  $A/Q$  values of the recoils. This was, however, found to be too energy consuming due to the windows the recoils had to be transmitted through in order to pass the PSAC. A large energy loss leads to a reduction of the  $Z$  resolution in the IC. Hence the PSAC was replaced with a Micro Channel Plate (MCP). The MCP is used at the  $A/Q$  dispersed focal plane and is able to run at much higher count rates than the PSAC. It is useful when determining, and hence optimising, the settings for the RMS; the knobs. It is also useful for checking that the recoils that we are interested in, i.e. the part of the beam with desired mass-to-charge ratio, actually enters the IC and is detected at the focal plane. However, due to energy losses the MCP is removed after the settings have been optimised. The position of the recoils inside the IC, i.e. , the mass-to-charge ratio is instead determined by a delay arrangement (see Sec. 1.4.2).

### 1.4.2 The Ionisation Chamber

An IC consists of a chamber filled with a particular gas that becomes ionised, or excited, when a charged particle moves through it. In each ionisation an ion-electron pair is created and, due to the electric field that is caused by the presence of an anode and a cathode, these charged particles will start to move. As the positive ions move towards the cathode and the electrons move towards the anode the net flow of charged particles creates an electric current, a signal that makes it possible to detect the incidenting particles. Furthermore, a given volume of gas that is constantly radiated with charged particles will have a constant ionisation rate. Hence if the recombination of ions is negligible and all the charges are collected the produced current will be proportional to the rate at which the gas is ionised. This will make it possible to determine the energy of the incoming particles.

In this experiment a position sensitive split-anode ionisation chamber filled with iso-butane gas at a pressure of 16.5 torr was used. It was placed at the mass separated focal plane at the very end of the RMS. The ion chamber is operated in pulse mode which means that each charged particle that enters the chamber will give rise to a separate output signal. The split anode (Fig. 1.4) makes it possible to determine three separate energy losses. These will vary depending on  $Z$  of the incidenting ion. The currents from the ionisations that will give the energy loss measurements are collected from the three parts of the anode. The first two parts are 50 mm long and the last section of the anode is 202 mm long [5]. The total energy loss from the ions may be determined by adding the losses from the three different sections of the anode. The pressure is chosen such that all ions deposit almost equal amounts of energy in the IC.

The IC is segmented into eight sections. This is useful in cases of high counting rates where this can prevent pile-up and hence minimise signal degradation. The sections can, however, be connected and used together as if the chamber was in fact not segmented. This was done in the case of our experiment.

Inside the ionisation chamber is a Frisch grid, which prevents the output pulse amplitude to be dependent on the vertical position of the ionisation. Through the use of, for example, an external collimator all the ionisations take place between the grid and the cathode inside the chamber, Fig. 1.6. The positive ions will drift to the cathode as per normal and the electrons will use the grid, which is kept fairly transparent to electrons, as an intermediate potential. The electrons hence drift from their initial position towards the grid and because of the construction of the circuit no output will be produced until they have passed it. However, when electrons are drifting between the grid and the anode a signal voltage is slowly produced. This increases as the electrons move closer. Since each electron moves the same distance between grid and anode, (in this setup this distance is 120mm [5]), the output signal amplitude will be independent of where the ion-electron pair was produced in the gas.

The horizontal position of the recoils inside the IC, i.e., their mass-to-charge ratio  $A/Q$ , is determined with a position-sense grid. The construction is fairly simple: When the recoils ionise the gas in the IC two signals will be sent from the point of ionisation. One signal travels to the right side of the IC and one to the left side. The signals travel through an electric circuit with evenly distributed delays. The time difference between receiving the right hand signal and the left hand signal will then give a determination of the position for the ionisation.

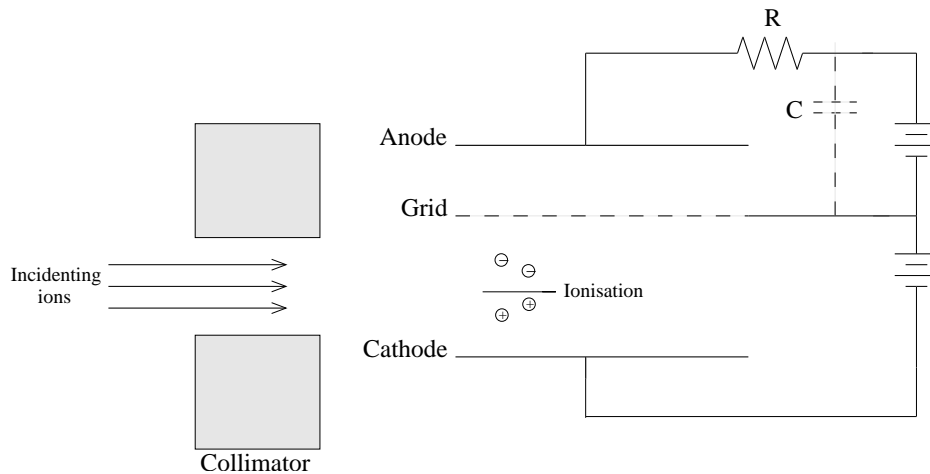


Figure 1.6: A schematic drawing of an ionisation chamber with a Frisch grid [6].



# Chapter 2

## Data Handling

During the running of the experiment the beam time is divided into small, so called runs for safety reasons; if something happens during the experiment not too much beam time should be wasted. The division is also handy during the preparations as it makes it possible to compare the effect of the eventually different settings of the equipment. Some of the runs from the preparatory beam time are used in the analysis. These are included in order to increase the statistics.

This chapter aims to briefly describe the preparatory work; the data sorting and calibrations required for the analysis.

### 2.1 Data Sorting

Throughout the running of the experiment data is collected and via the use of triggers one may determine which parts of the collected data should be saved. A section of the data is shown below. It is written in hexadecimal and each event, i.e., each produced excited recoil is separated by a string of “ffff ffff”. The data below contains two complete events and the very start of a third.

```
ffff ffff 817a 0751 83ba 0465 83b9 03f8
83b8 0488 83bf 08a4 83b7 041d 800d 6200
807f 1109 80e3 063d 81a4 0215 81bf 0004
ffff ffff 83ba 0256 83b9 016e 83b8 02a7
83bf 0872 83b7 02a9 800d 6200 807f 161b
80e1 0507 80e2 050d 80e3 059f 81a4 02d2
8011 3200 8087 0caf 80e9 055c 80eb 05ea
80ec 055a 81aa 0045 81ab 0137 81c1 0002
ffff ffff 817a 0744 83ba 0491 83b9 046c
```

The data is written in a structure consisting of words, each of which contains four digits. The words are connected two by two where the first always starts with an eight. The three following digits provide the identification number corresponding to a certain parameter such as, for example, Ge energy, Ge time, or RMS data. The second word gives the value of the parameter.

Off-line the data is read event-by-event from the DVD and simultaneously checked to see if the data is valid and can be used or not. The Ge detectors should, for example, have both time and energy for each crystal and the RMS needs to have four

parameters: one for each section of the anode plus a position of the recoil in order to be useful for the analysis. If the parameters are not complete the  $\gamma$ -ray or recoil is disregarded. When this check has been performed the different parameters must be aligned and calibrated to give good results when the entire experiment is sorted and analysed.

## 2.2 Calibration and Alignment of the Ge-Detectors

I will only briefly mention the different calibrations, corrections, and alignments made for the Ge detectors and the reason for performing the different steps. To get a more detailed description of these steps I refer to the Master thesis of Emma Johansson [1].

- **Energy calibration:** As calibration sources  $^{152}\text{Eu}$ ,  $^{133}\text{Ba}$ , and  $^{88}\text{Y}$  were used. The three radioactive isotopes have peaks at well defined energies. The 44 Ge detectors and the 33 side channels can hence be energy calibrated.
- **Time alignment:** The time spectra for all the crystals in all the runs have to have the recoil- $\gamma$  part placed on top of each other so that all signals from a certain time interval originate from recoils and  $\gamma$ -rays that are correlated. In the same way it may be desirable to look at the  $\gamma\gamma$  correlation peak.
- **Add-back:** The more energetic  $\gamma$ -rays are the more probable it is for them to be Compton scattered in a Ge detector. A scattered  $\gamma$  may deposit its energy in more than one crystal within the same clover detector and will then be detected as several less energetic  $\gamma$ -rays instead. Add-back gives a possibility to add together signals from several crystals in one clover if they hit the detector within a certain time interval and if they deposit a reasonably high energy. This correction will both reduce low energetic noise and increase the number of detected  $\gamma$ -rays at higher energies.
- **Efficiency calibration:** An intrinsic quality of the Ge detectors is that they do not detect  $\gamma$ -rays of different energies equally efficient. The efficiency calibration is done to make up for this fact.
- **Doppler correction:** It is possible to determine the velocity of the recoils and via that make Doppler corrections to account for the Doppler shift and broadening of the peaks, both in the crystals and in the side-channels. First a rough correction was made using the same velocity for all the recoils but later a better determination of  $\beta$  ( $=v/c$ ) was made where  $\beta$  was described as a function of the total energy of the recoil determined by the IC.

## 2.3 Calibration of the Ionisation Chamber

An ion that incidents into the IC will, as mentioned in Sec. 1.4.2, deposit different amounts of energy in the three regions defined by the three parts of the anode. The amount of energy lost to each anode is mainly dependent on the number of protons

of the ion. By looking at the three different energy losses as a function of the total energy of a recoil, it is obvious that the energy losses also are strongly dependent of the ion's total energy. Naturally it is desirable to calibrate the IC and to look at the energy losses independent of the total energy of the ions, according to the Bethe-Bloch formula.

I choose to look at  $dE1$ ,  $dE2$ ,  $dE3$ ,  $dE1+dE2$ ,  $dE1-dE3$  and  $dE1/dE3$ . All six are plotted as a function of the total energy of the recoil. The goal is to choose the part of the IC or the energy loss function, listed in Table 2.1, that gives the best  $Z$  separation. This will be described in more detail in Sec. 2.4.

Energy loss function #1	$\Delta E1 + \Delta E2$
Energy loss function #2	$\Delta E1 - \Delta E3$
Energy loss function #3	$\Delta E1/\Delta E3$

Table 2.1: The energy loss functions.

For the  $A = 61$  isotopes used here it is easiest to start the re-calibration by just looking at  $^{61}\text{Cu}$  and  $^{61}\text{Zn}$  and then apply the result from these re-calibrations to fit all the recoils incidenting into the IC. The two isotopes can be selected since if a recoil has emitted a  $\gamma$ -ray with an energy of 124 keV this recoil is most likely  $^{61}\text{Zn}$ , because the energy difference between the  $5/2^-$  and the ground state in this element is 124 keV. The same applies for the 970 keV transition in  $^{61}\text{Cu}$ .

It seems logical to calibrate with respect to  $^{61}\text{Zn}$  recoils as  $^{61}\text{Zn}$  has the intermediate mass-to-charge ratio of the three nuclei with  $A = 61$  and will hence have its IC spectra placed at an intermediate position.  $^{61}\text{Zn}$  has a somewhat smaller cross-section than  $^{61}\text{Cu}$  which is unfortunate but the statistics is still good enough to use for the calibration. Figure 2.1 shows the plot for  $^{61}\text{Zn}$  for one of the energy loss functions as it looks before any corrections are made. The energy dependence is obvious.

The first step in making the energy loss independent of the recoil's energy is to cut energy sections of the 2D plots (I will refer to them as blobs from here on) and project them onto the  $y$ -axis one by one. The positions of the peaks from the different sections may then be fitted to a linear function, i.e., a line running straight through the blob and through which it can be rotated into horizontal position. In order to perform the rotation one will first have to find the  $x$  and  $y$  coordinates around which the rotation can be made, also the angle of rotation has to be determined. When rotating it is also important to make sure that the blob will be placed at a mean height compared to the lowest and the highest value of  $y$  of the blob. The rotated plot can be seen in the upper part of Fig. 2.2. When looking at this blob it can be seen that it is not completely straight nor smooth. This impression is further confirmed if one, once again, projects it in sections onto the  $y$ -axis. The

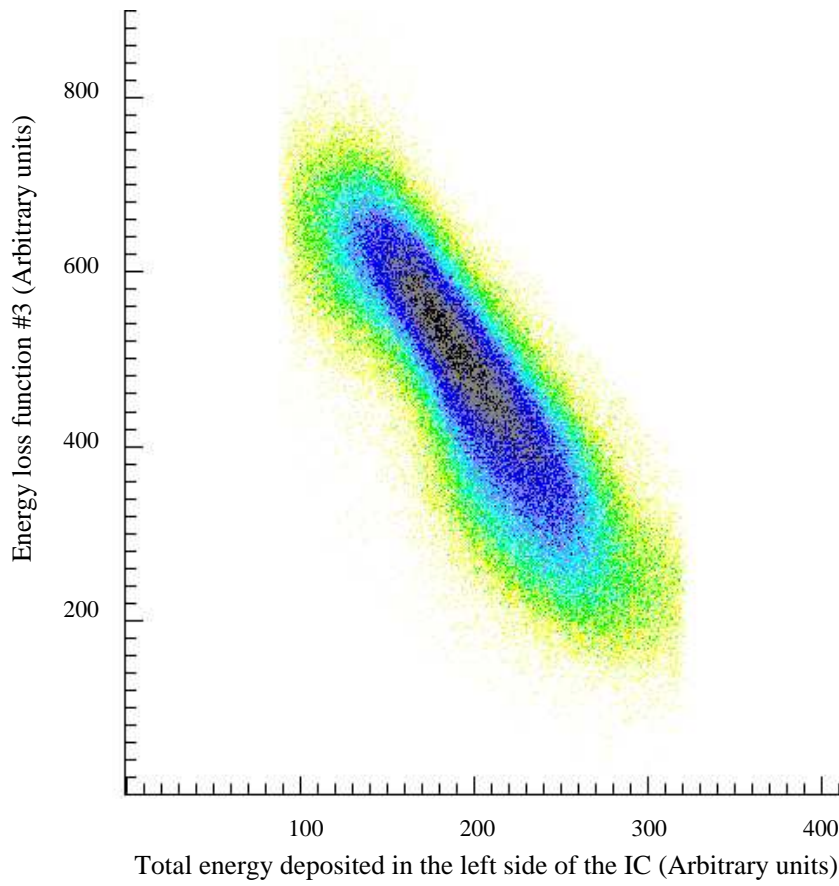


Figure 2.1: Uncorrected plot of energy loss function #3 versus total energy deposited in the left side of the IC. The dependence between the two quantities is obvious.

obtained peaks should then fit on top of each other but this is not the case. This indicates that there is some kind of intrinsic correlation between the  $x$  and  $y$ -axis in the rotated blob which must be corrected for. The positions of all the projected peaks are yet again determined and fit to a polynomial of suitable degree. Degree two or three was generally chosen, and the blob can now be completely straightened out. The final result of the corrections can be seen in the lower part of Fig. 2.2.

It is possible to double check the accuracy of the corrections by once again projecting the two dimensional spectra, in sections, onto the  $y$ -axis. The projected peaks should be placed on top of each other. It is especially important that the right side of the peaks are adjusted properly as  $^{61}\text{Ga}$  will be found to the right of the  $^{61}\text{Zn}$  peak.

When all these corrections are made for the  $^{61}\text{Zn}$  recoils in the six different plots of energy losses and energy loss functions the procedure can be applied to the selected  $^{61}\text{Cu}$  recoils, and in the end all recoils. When looking at the six plots it is easy to see that in any plot the blob will be placed at almost the same energy no matter what mass the recoils in the blob has. Hence the transformations in rotating and straightening of the blob found for  $^{61}\text{Zn}$  must be used for all the recoils as for any one point there can be only one valid mathematical transformation.

When all the corrections are made the signals from the three parts of the anode

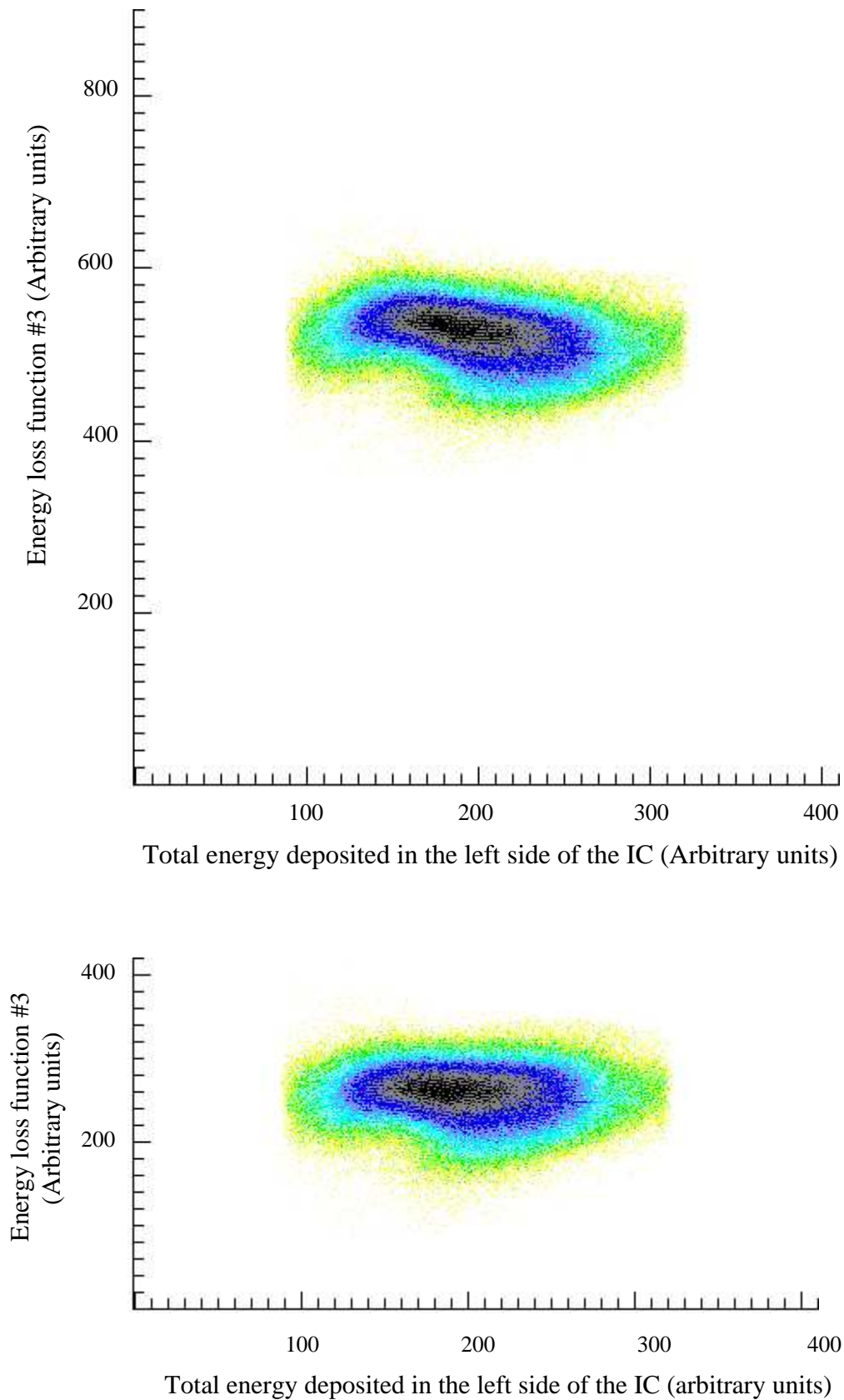


Figure 2.2: (Top) The blob is here rotated into horizontal position. By looking at the very core of the blob where the intensity is at its highest (here coloured in black) it is obvious that the blob is not completely straight yet. (Bottom) Completely corrected blob with no dependence between the quantities on the  $x$  and  $y$ -axis.

and the position in the IC will have to be shifted to fit on top of each other for all the runs throughout the experiment. In practise this means that the recoils of a specific mass and charge state always will end up at the same place at the  $A/Q$  dispersed focal plane even if the RMS settings may change slightly during the run time. This is important for the analysis since it is very useful to be able to select certain masses or select only the recoils, not the beam or scattered parts of it, that incidents into the IC.

## 2.4 Optimising the $Z$ Separation

The goal is to find the best  $Z$ -resolution in the IC by using the energy losses in the different parts of the detector. It has been standard to use the  $Z$ -separation obtained in a plot of energy loss function #1 vs. total energy loss in the IC but nothing indicates that this in fact gives the best separation. On the contrary it is known that for a given charge state the energy loss in the first part of the IC will increase with increasing  $Z$ . Simultaneously, the loss in the third part will decrease and the loss in the second part remains approximately constant. From this one may assume that an energy loss function that combines  $dE1$  and  $dE3$  could give the best result.

By trial and error it is found that a better result is obtained if we increment spectra of an energy loss function vs. total energy loss and then make the corrections mentioned in Sec. 2.3 than if the corrections of the three parts are done separately and the energy loss function is calculated and incremented afterwards.

To determine the best  $Z$  resolution the separation between  $^{61}\text{Zn}$  and  $^{61}\text{Cu}$  recoils are studied. The entire 2D spectra for which the corrections were made in Sec. 2.3 can be projected out on the  $y$ -axis, this is done for all the six plots. By looking at these projections, here referred to as IC spectra, one can see a shift in position between  $^{61}\text{Zn}$  and  $^{61}\text{Cu}$ , (c.f. Figs. 3.1 and 3.2). Ideally the separation between the IC spectra is large and the FWHM is small. By dividing the size of the peak separation with the FWHM of the peaks a so called figure of merit is obtained. The larger the figure of merit the better the  $Z$ -resolution.

It is obvious from the data that the three energy loss functions listed in Table 2.1 are far superior in resolution compared to when only looking at the energy losses separately. The best separation is here found when using energy loss function #3. This can, however, be investigated further once a peak of  $^{61}\text{Ga}$  has been found. This is described in Sec. 3.2.1.

# Chapter 3

## Data Analysis and Results

### 3.1 The Recoil- $\gamma$ Matrix

The construction of the detector system with CLARION and the RMS followed by the IC makes it possible to investigate only  $\gamma$ -rays emitted in coincidence with a detected recoil in the IC, i.e., only  $\gamma$ -rays emitted by the recoils that are detected and identified in the IC.

The recoil- $\gamma$  matrix is a 2D spectrum in which the previously chosen energy loss function #3, which gives the best  $Z$  resolution, is plotted against the  $\gamma$ -ray energy. It is possible to include only recoils with a specific mass-to-charge ratio in the matrix by gating at the  $A/Q$  dispersed focal plane. Since  $^{61}\text{Ga}$  is of prime interest in this thesis the recoil- $\gamma$  matrix comprises only recoils of  $A = 61$ . These incident on the left side of the IC with charge state  $Q = 18$  (c.f. Fig. 1.5).

The recoil- $\gamma$  matrix may be projected out on either axis, giving a  $\gamma$ -ray spectrum if projected on the  $x$ -axis and an IC spectrum if projected onto the  $y$ -axis. The two cases will be considered separately.

#### 3.1.1 The IC Spectrum

As mentioned in Sec. 1.4.2 the energy losses in the three parts of the IC depend on the charge of the incidenting nuclei. This is good to keep in mind as it allows separation of different elements, with different  $Z$ , by their value of the energy loss function.

If projecting the recoil- $\gamma$  matrix onto the  $y$ -axis an IC spectrum will be obtained. An IC spectrum is simply a curve where intensity is plotted against energy loss function. When projecting the entire recoil- $\gamma$  matrix onto the  $y$ -axis the spectrum looks rather like a smooth curve but is in fact a combination of three closely placed smaller curves, each with their maxima placed on different values of energy loss function #3. The three small curves belong to  $^{61}\text{Cu}$ ,  $^{61}\text{Zn}$ , and  $^{61}\text{Ga}$ . By just looking at the entire matrix projected onto the  $y$ -axis it is impossible to determine at which values of energy loss function #3 the different elements will have their maximum. To investigate this one will instead have to find a rather strong  $\gamma$ -ray transition from  $^{61}\text{Cu}$  and  $^{61}\text{Zn}$  and look at these separately. Via the program it is possible to make a  $\gamma$  gate, i.e., to pick out only the recoils that have emitted a  $\gamma$ -ray with the energy of the chosen peak and project these onto the  $y$ -axis. Hence by only

projecting the nuclei that have emitted a  $\gamma$ -ray of 970 keV, a strong transition in  $^{61}\text{Cu}$ , one may obtain an IC spectrum containing only  $^{61}\text{Cu}$  recoils (Fig. 3.2). The same can be done with  $\gamma$ -rays of 124 keV to get the IC spectrum from  $^{61}\text{Zn}$ .

### 3.1.2 The $\gamma$ -Ray Spectrum

As mentioned earlier the  $\gamma$ -ray spectrum is obtained by projecting the recoil- $\gamma$  matrix onto the  $x$ -axis. If the entire matrix is projected the spectrum will naturally contain peaks from transitions from both  $^{61}\text{Cu}$ ,  $^{61}\text{Zn}$ , and  $^{61}\text{Ga}$ , since they all are present in the  $A = 61$  matrix.

As mentioned above it is possible to partly separate different elements by their value of the energy loss function. This can also be seen in Fig. 3.1 and is basically

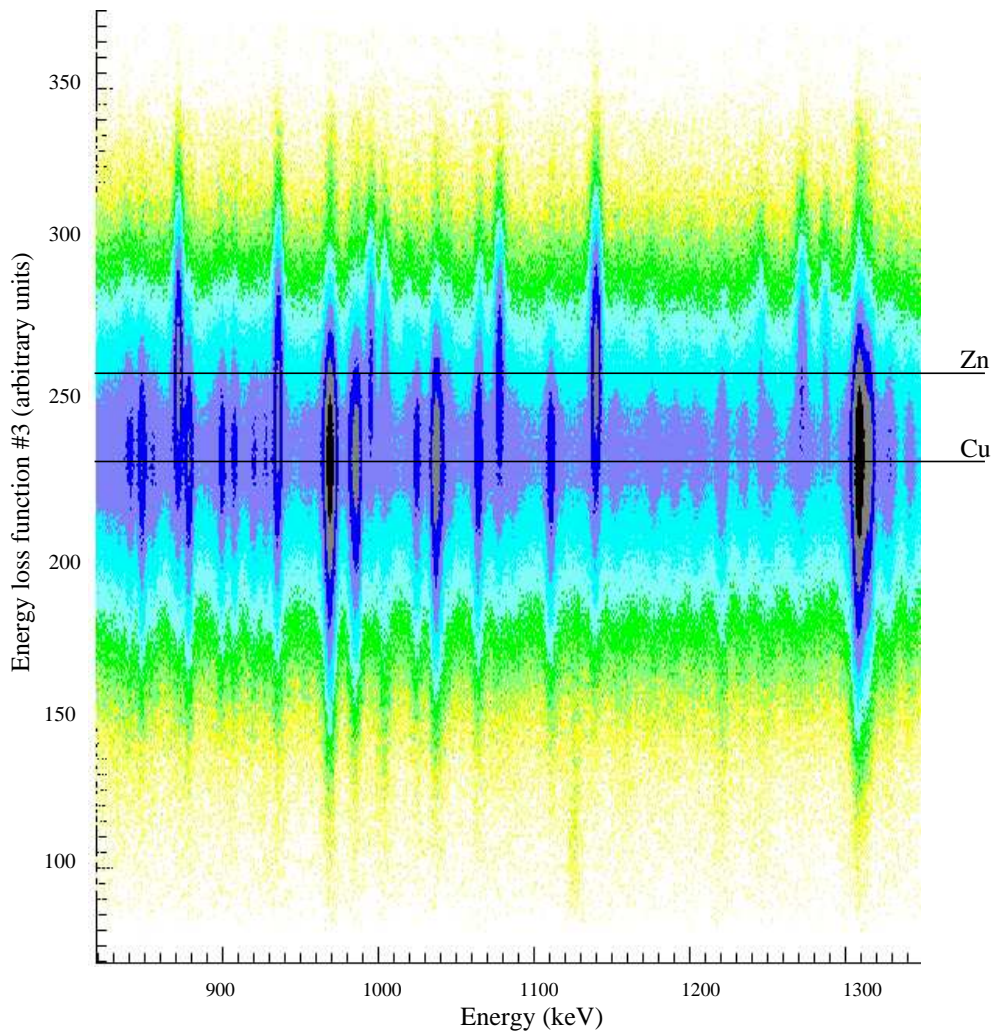


Figure 3.1: A part of the recoil- $\gamma$  matrix gated on recoils of  $A = 61$ . Some  $\gamma$ -ray energies have their maximum intensity placed higher up on the  $y$ -axis than others. This is due to the fact that  $^{61}\text{Zn}$  and  $^{61}\text{Cu}$  have different charges when incidenting into the IC. Hence they emit different amounts of energy in the three different parts of the IC, respectively. The energy loss function will therefore have different values depending on which recoil emits the  $\gamma$ -ray. The two horizontal lines indicate the peak positions of the maximum of the IC spectra for  $^{61}\text{Zn}$  and  $^{61}\text{Cu}$ , respectively.

the reversed procedure performed in Sec. 3.1.1. By introducing a restriction on the value of the energy loss function one obtains  $\gamma$ -ray spectra that contain mainly (but not exclusively)  $\gamma$ -rays originating from excited states in one particular isotope. I have here chosen to call these “raw spectra”.

By looking at the IC spectra obtained in Sec. 3.1.1 one can determine an interval for the gate, i.e., a region of energy loss function #3, where the incidenting nuclei are mainly  $^{61}\text{Cu}$ . In this case the gate is set from channels 210 to 225. The gate is illustrated in Fig. 3.2. In Fig. 3.3 the green curve shows the raw  $\gamma$ -ray spectrum. It is obvious that the spectrum contain  $\gamma$ -rays originating from other nuclei than  $^{61}\text{Cu}$ . For example, the 124 keV peak from  $^{61}\text{Zn}$  is fairly strong. In the same way a raw  $^{61}\text{Zn}$  spectrum, Fig. 3.4, will be obtained by gating between channels 255 to 270. When choosing the gate for  $^{61}\text{Zn}$  one must, however, keep in mind that somewhere to the right of the IC  $^{61}\text{Zn}$ -spectrum the  $^{61}\text{Ga}$  spectrum must be placed. Hence one should avoid to put the gate too far to the right as it is vital to minimise the amount of  $^{61}\text{Ga}$  nuclei in it.

To determine a gate for  $^{61}\text{Ga}$  is slightly harder than for  $^{61}\text{Zn}$  and  $^{61}\text{Cu}$  as we do not have an IC spectrum for this element yet. However, it is easy to see in,

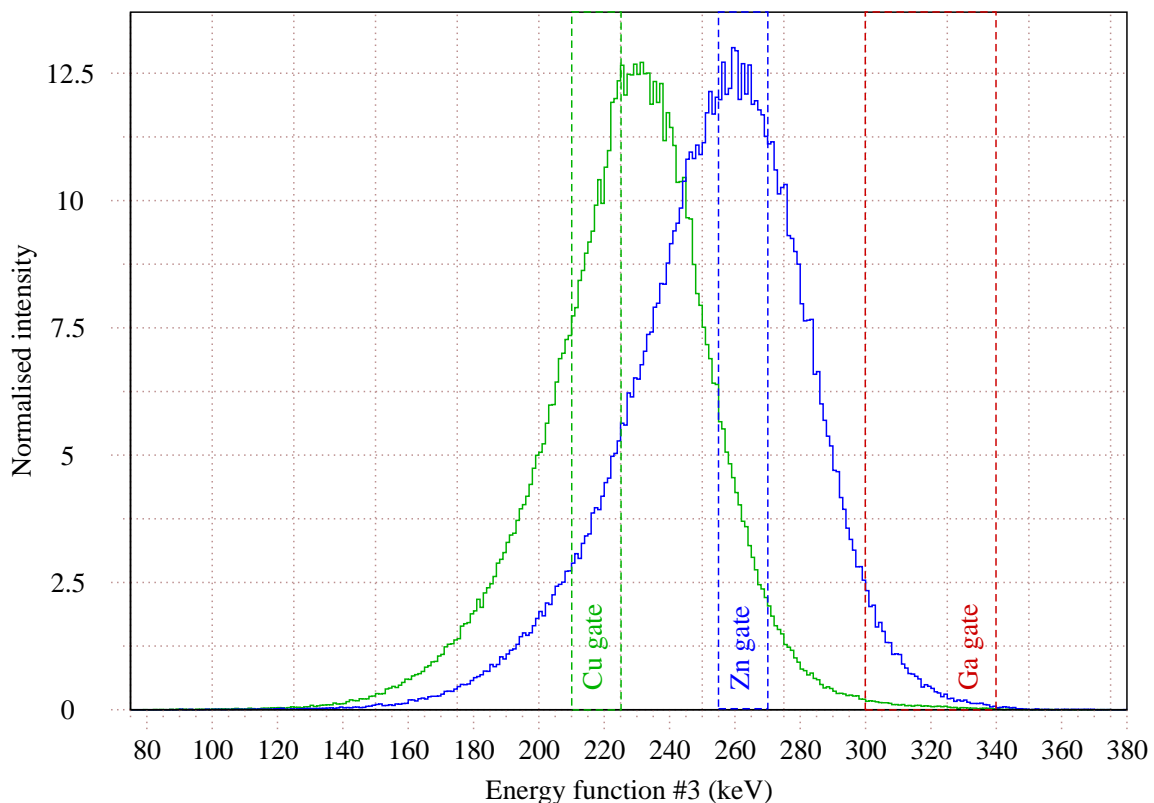


Figure 3.2: The IC spectra from  $^{61}\text{Zn}$  and  $^{61}\text{Cu}$ , obtained by choosing recoils via strong known transitions. The gates for projecting the “raw”  $^{61}\text{Cu}$ ,  $^{61}\text{Zn}$ , and  $^{61}\text{Ga}$   $\gamma$ -ray spectra are indicated. The  $^{61}\text{Ga}$  gate is a lot bigger than the other gates. This is due to the fact that there are only these three elements present within the used mass gate. Hence there is no direct risk apart from additional background when increasing the gate to the right, and one needs as much statistics as possible.

for example, Fig. 3.2 that the IC spectrum will have its peak maximum placed at different values of energy loss function #3 depending on the  $Z$ -value of the peak. One can hence determine the approximate position of the peak maximum for  $^{61}\text{Ga}$ .  $^{61}\text{Cu}$ , with  $Z = 29$ , has its maximum at channel  $\sim 230$  and  $^{61}\text{Zn}$ , with  $Z = 30$ , has its at channel  $\sim 260$ . Hence one would expect that  $^{61}\text{Ga}$ , with  $Z = 31$ , would have its peak maximum placed at channel  $\sim 290$ . In an attempt to avoid too many  $^{61}\text{Zn}$  recoils in the gate I chose it between channel number 300-330. This is, however, just a preliminary choice which will be improved in Sec. 3.2.1. In Fig. 3.2 the final gate choice is shown.

To create spectra with  $\gamma$ -rays only originating from recoils of a particular isotope it is best to start with  $^{61}\text{Cu}$  as this isotope has by far most statistics. The ‘‘clean’’ spectrum is obtained by subtracting a fraction of the raw  $^{61}\text{Zn}$  spectrum from the raw  $^{61}\text{Cu}$  spectrum. In order to do this one has to normalise the two spectra first. The subtraction will then remove the  $^{61}\text{Zn}$  peaks from the  $^{61}\text{Cu}$  spectrum. Simultaneously the intensity of the  $^{61}\text{Cu}$  peaks will decrease slightly. It is, however, not always completely safe to just subtract one spectrum from another. Small shifts in energy position will cause difficulties and in some cases the best method is actually to subtract several raw  $^{61}\text{Zn}$  spectra from the raw  $^{61}\text{Cu}$  spectrum. These three spectra will, when used together, remove the unwanted peaks more efficiently than one single spectrum if they are shifted slightly in energy with respect to each other. Using trial and error allows to obtain a spectrum which does not contain any  $^{61}\text{Zn}$  peaks at all. The ‘‘clean’’  $^{61}\text{Cu}$  spectrum can be seen in Fig. 3.3. In the same way a clean  $^{61}\text{Zn}$  spectrum is obtained, shown in Fig. 3.4. The method described above works fine for  $^{61}\text{Zn}$  and  $^{61}\text{Cu}$  as the  $^{61}\text{Ga}$  nuclei are so few in comparison and will not interfere. In the raw  $^{61}\text{Ga}$  spectrum at the other hand most of the peaks will belong to  $^{61}\text{Cu}$  and  $^{61}\text{Zn}$  and the simple method cannot be applied in this case. Instead a combination of the raw spectra from  $^{61}\text{Zn}$  and  $^{61}\text{Cu}$  must be used to weigh the subtraction of the two isotopes from the raw  $^{61}\text{Ga}$  spectrum. The weighting factors  $a$  and  $b$  can be calculated in the equations below:

$$a * I(124(^{61}\text{Cu})) + b * I(124(^{61}\text{Zn})) = -I(124(^{61}\text{Ga})) \quad (3.1)$$

$$a * I(970(^{61}\text{Cu})) + b * I(970(^{61}\text{Zn})) = -I(970(^{61}\text{Ga})) \quad (3.2)$$

Where, for example,  $I(970(^{61}\text{Zn}))$  refers to the intensity of the 970 keV peak in the raw  $^{61}\text{Zn}$  spectrum. By measuring the intensities of the 970 and the 124 keV peaks in the raw spectra from both  $^{61}\text{Cu}$  and  $^{61}\text{Zn}$  one will be able to determine the coefficients  $a$  and  $b$ . Using these results one obtains a pure  $^{61}\text{Ga}$  spectrum by adding and subtracting the  $^{61}\text{Cu}$  and  $^{61}\text{Zn}$  components from the raw  $^{61}\text{Ga}$  spectrum. The method involving the use of additional spectra slightly shifted in energy may also be applied in this case to improve the outcome of the  $^{61}\text{Ga}$  spectrum. It is, however, important to keep in mind that since there are relatively few  $^{61}\text{Ga}$  nuclei the final spectrum will be less clear and much more noisy than the spectra obtained for  $^{61}\text{Cu}$  and  $^{61}\text{Zn}$ . The  $^{61}\text{Ga}$  spectrum is shown, split in two parts, in Fig. 3.5. A strong transition at 271 keV can clearly be seen in this spectra and it is the first time any transition from  $^{61}\text{Ga}$  has been determined.

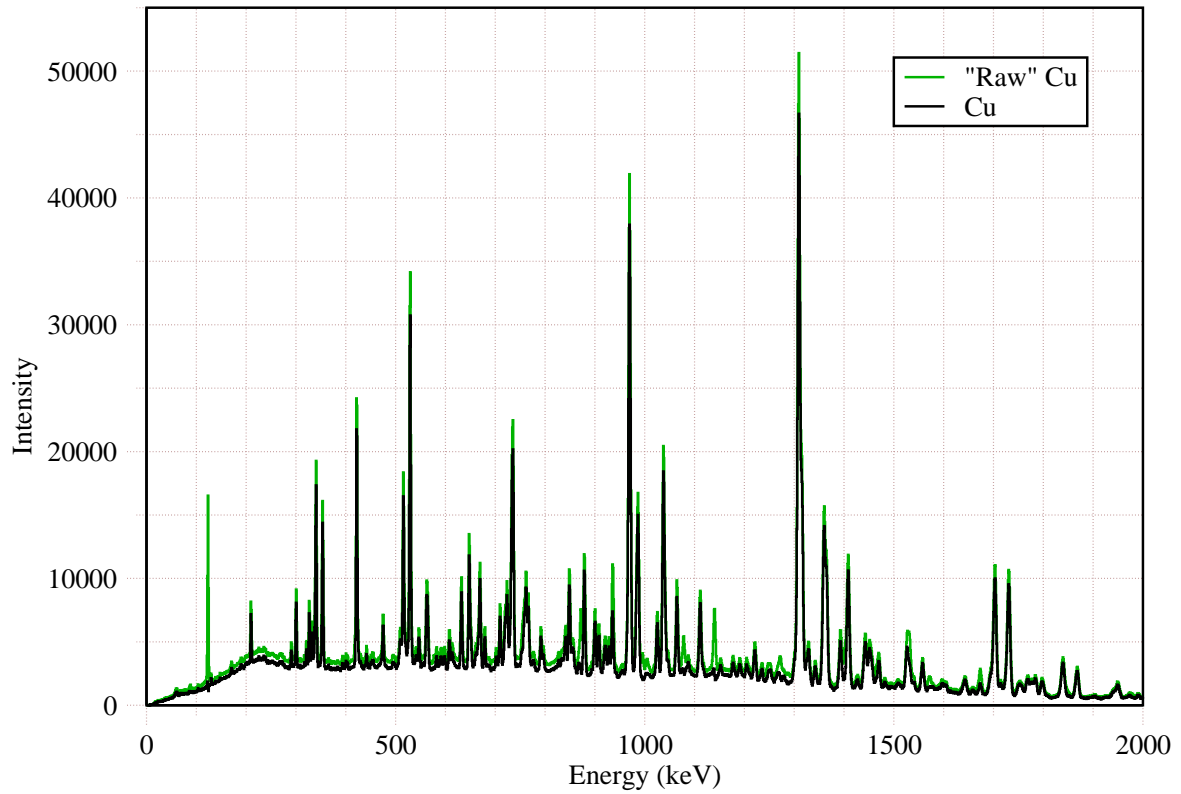


Figure 3.3: Spectra of  $^{61}\text{Cu}$ . The raw spectrum is shown in green and the black spectrum contains only  $\gamma$ -rays from transitions in  $^{61}\text{Cu}$ .

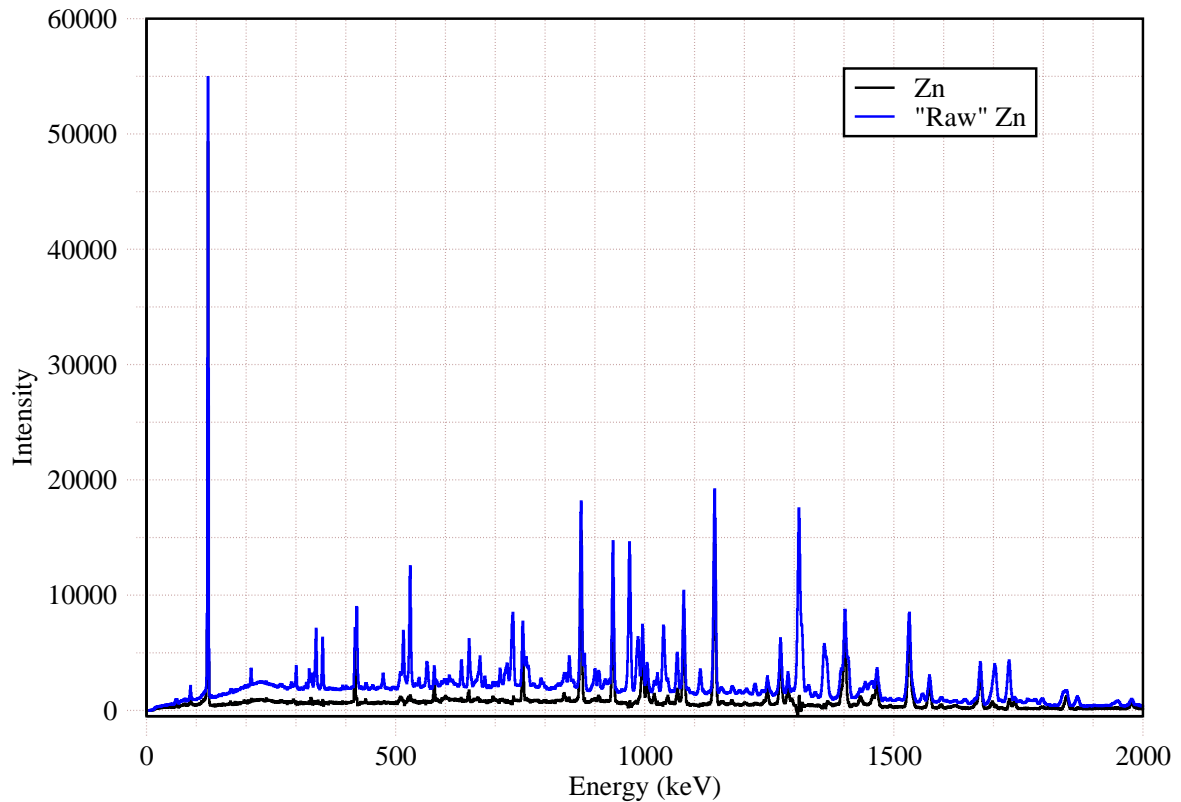


Figure 3.4: Spectra of  $^{61}\text{Zn}$ . The raw spectrum is shown in blue and the black spectrum contains only  $\gamma$ -rays from transitions in  $^{61}\text{Zn}$ .

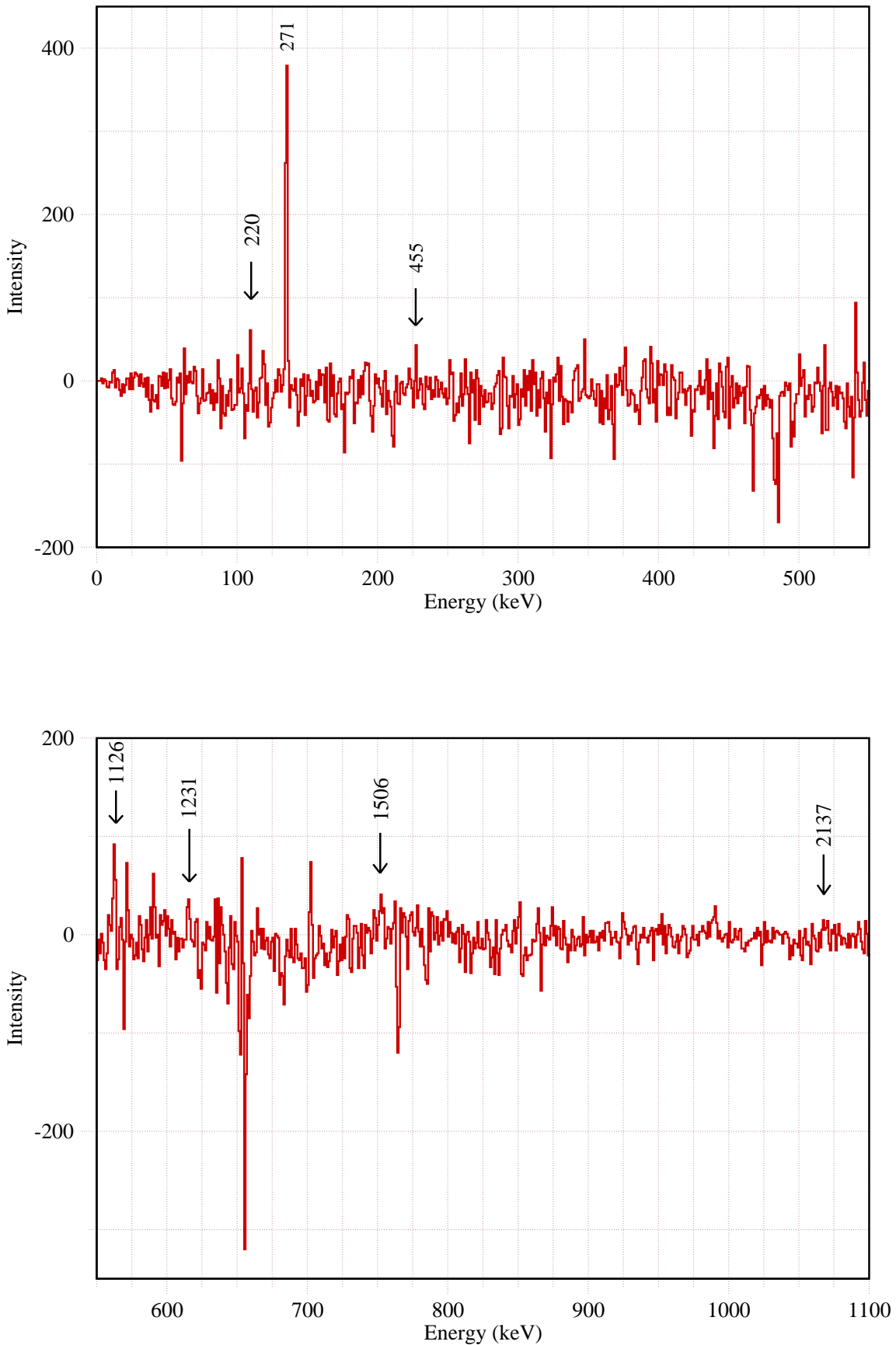


Figure 3.5: “Clean” spectra of  $^{61}\text{Ga}$ . The spectra are somewhat noisy and difficult to use for final conclusions about the existing transitions. The 271 keV peak is, however, strong and obvious as a candidate for a transition in  $^{61}\text{Ga}$ .

The spectrum is, however, not really clear enough to give complete confidence about further  $\gamma$ -ray transitions in the  $^{61}\text{Ga}$  nucleus but can rather be used as a hint or confirmation of transitions that are investigated through other methods.

## 3.2 Transitions in $^{61}\text{Ga}$

When finding transitions the first step is to confirm the chosen  $Z$ -separation and optimise the size and position of the chosen gate. The next step is to find transitions from  $^{61}\text{Ga}$  and confirming them by incrementing an IC spectrum for all the transitions separately.

The decay scheme may then be created and drawn with the help of the recoil-gated  $\gamma\gamma$  matrix (see Sec. 3.2.4) and by comparing the transitions with those in  $^{61}\text{Zn}$ , the mirror nucleus of  $^{61}\text{Ga}$ .

### 3.2.1 Improving the $^{61}\text{Ga}$ Gate

As mentioned earlier it is important, since  $^{61}\text{Ga}$  nuclei are much rarer than both  $^{61}\text{Zn}$  and  $^{61}\text{Cu}$ , to choose a gate of  $^{61}\text{Ga}$  that contains as small amounts of the other isotopes as possible. The preliminary choice of the gate between channels 300-330 can be used to find a peak from  $^{61}\text{Ga}$ . By comparing the clean  $^{61}\text{Zn}$  spectrum with a spectrum containing both  $^{61}\text{Ga}$  and  $^{61}\text{Zn}$ , obtained according the procedure earlier mentioned, it is easy to see if there are any peaks belonging to  $^{61}\text{Ga}$  as these will only appear in the latter spectrum. Figure 3.6 shows an example of such a comparison. At 271 keV there is a very clear peak that very likely belongs to  $^{61}\text{Ga}$ . Knowing the position of one peak makes it easy to increment many spectra with different size and position of the  $^{61}\text{Ga}$  gate. These may then be compared to see which interval is superior for the choice of gate, i.e., which interval gives the  $^{61}\text{Ga}$  peak the highest intensity and cleanliness. To further confirm that the chosen energy loss function gives the best  $Z$ -resolution, spectra for a number of gates were incremented also for the two other energy loss functions and the best gate of each was compared so that the very best gate and energy loss function is used in the end. Energy loss function #3 still seems to be the best if using a gate between channels 300-340 (c.f. Fig. 3.2).

### 3.2.2 Finding Transitions

By using the optimised gate one can increment a new spectrum containing both  $^{61}\text{Zn}$  and  $^{61}\text{Ga}$  and use this to find more peaks. The peaks are found by comparing the clean  $^{61}\text{Zn}$  spectrum and the spectrum containing both  $^{61}\text{Zn}$  and  $^{61}\text{Ga}$ . All peaks present in the latter but not in the first are potential  $^{61}\text{Ga}$  peaks. One should, however, keep in mind that close to energies at which  $^{61}\text{Cu}$  has large peaks small peaks may appear due to subtraction difficulties. When comparing the two spectra a number of potential peaks were found, at 220, 271, 1126, 1231, 1506, and 2137 keV. The four figures 3.6, 3.7, 3.8 and 3.9 show different parts of the two spectra with normalised intensities. The promising transitions are marked. These transitions are also to some degree confirmed in the clean  $^{61}\text{Ga}$  spectrum. Figure 3.5 shows the  $^{61}\text{Ga}$  spectrum with the same peaks marked. It is good to keep in mind that a

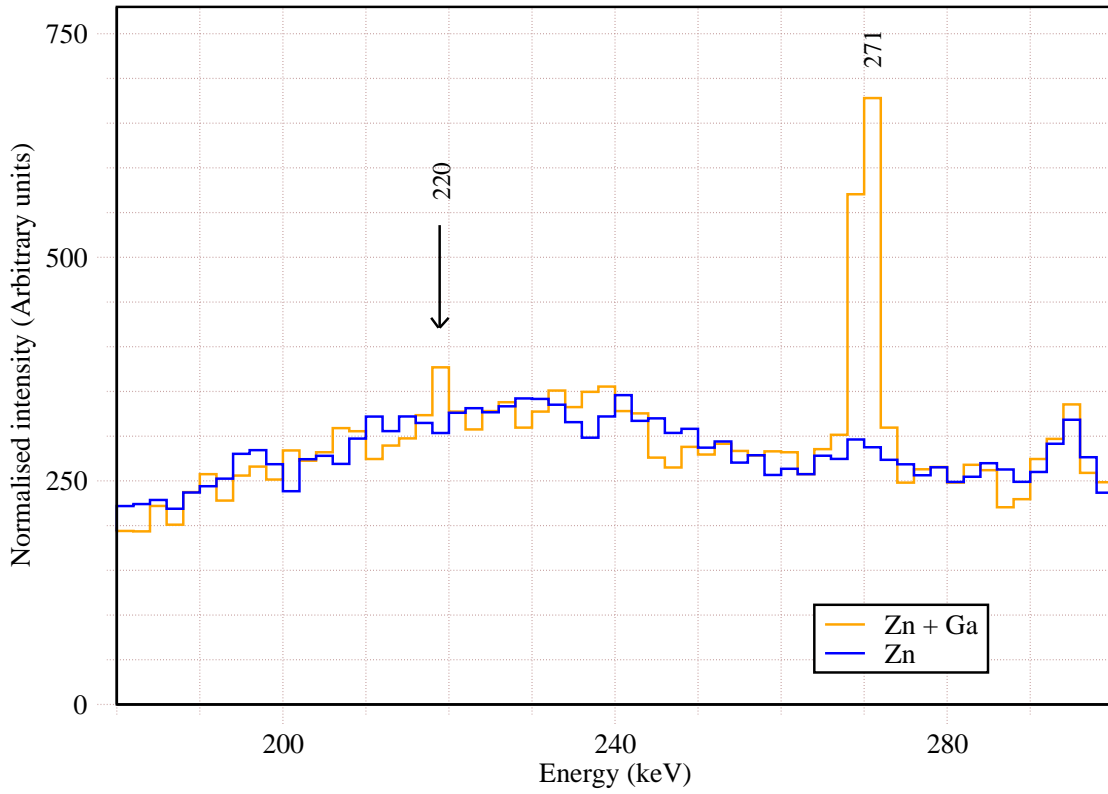


Figure 3.6: Normalised spectra of  $^{61}\text{Ga}+^{61}\text{Zn}$  (orange) and  $^{61}\text{Zn}$  (blue). Looking at both spectra makes it easier to find transitions only present in  $^{61}\text{Ga}$  nuclei.

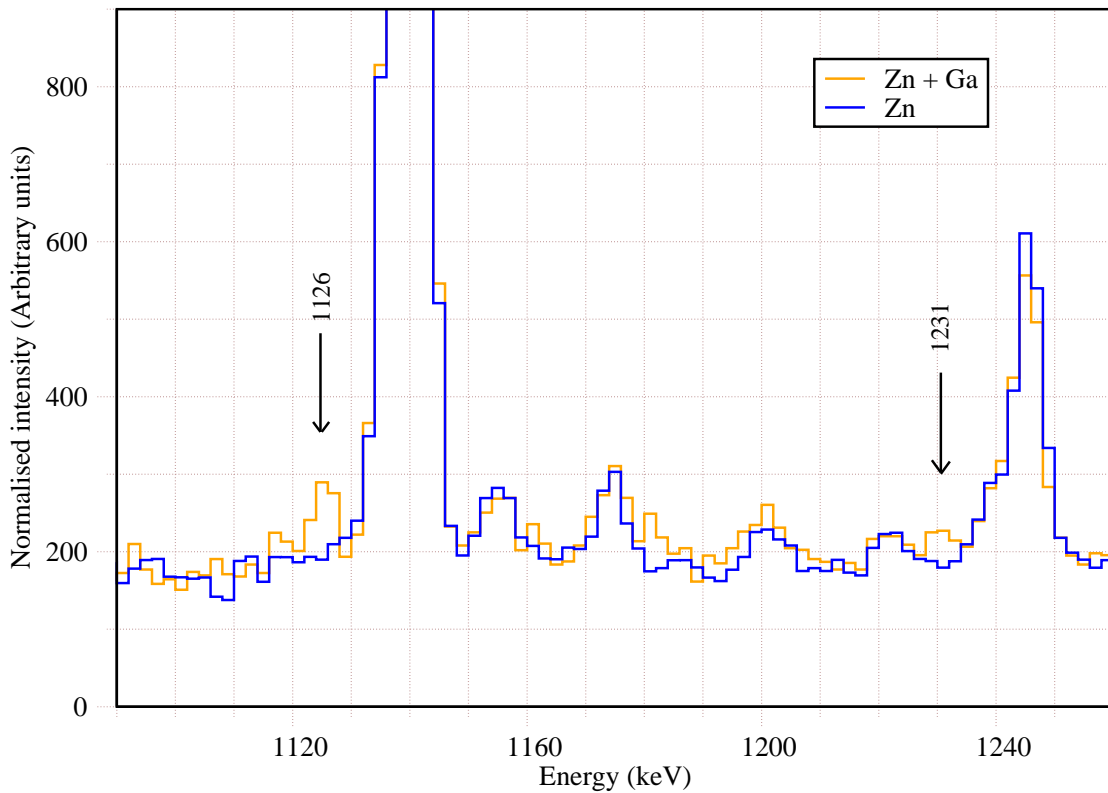
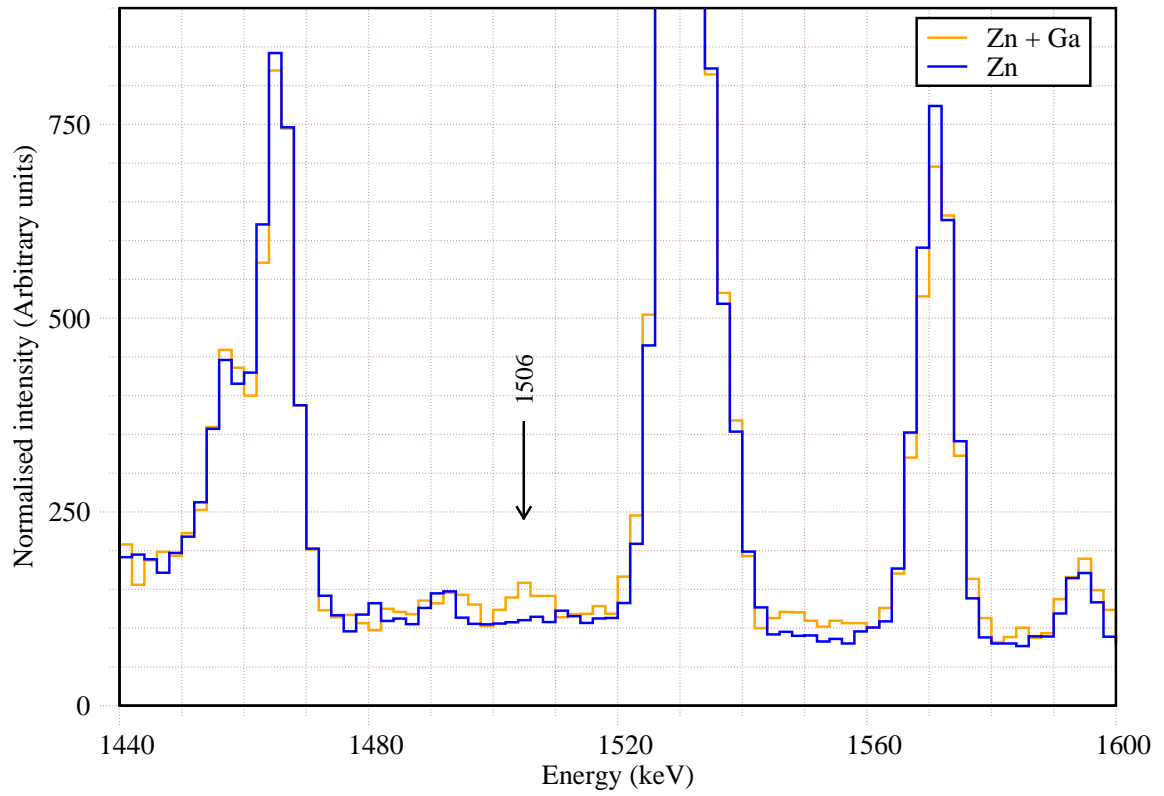
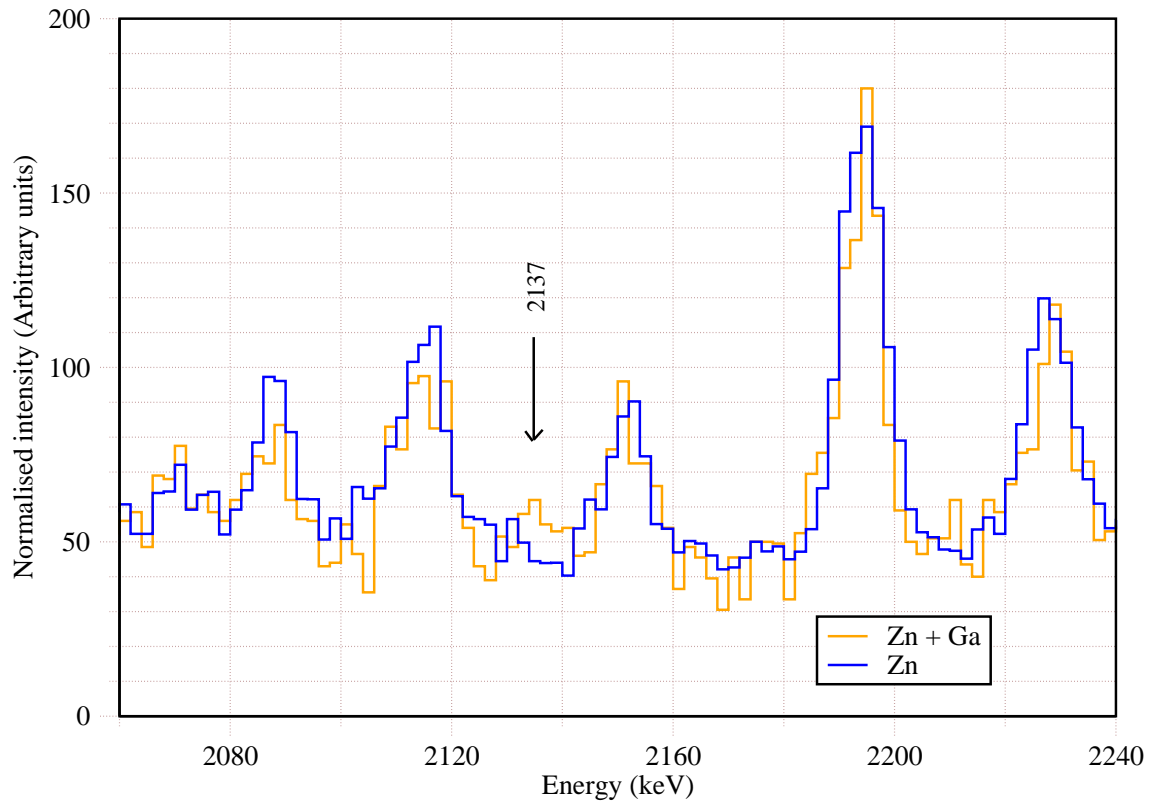


Figure 3.7: Same as Fig. 3.6 but different  $\gamma$ -ray energy regime.

Figure 3.8: Same as Fig. 3.6 but different  $\gamma$ -ray energy regime.Figure 3.9: Same as Fig. 3.6 but different  $\gamma$ -ray energy regime.

possible candidate has to have a width of a few keV. All peaks which are preceded with a dip in the spectrum or only have a width of one or two channels are likely to arise from subtraction difficulties mentioned earlier.

Looking at Fig. 3.5 there is a peak at 1978 keV that is of the right width and appears to be a promising transition in  $^{61}\text{Ga}$ . However, when comparing the spectrum containing  $^{61}\text{Ga}$  and  $^{61}\text{Zn}$  with the one containing only  $^{61}\text{Zn}$  one immediately realises that this is in fact not a very good candidate as  $^{61}\text{Zn}$  has a transition at the same energy.

### 3.2.3 Confirmation via IC Spectra

It is possible to find peaks by just comparing spectra and to confirm them via the clean  $^{61}\text{Ga}$  spectrum but this method is not good enough to prove that the found peaks actually belong to  $^{61}\text{Ga}$ . In order to make a real proof to which isotope the peak belongs to one will have to look at the spectra from the IC again.

It has already been mentioned that if gating at a peak one may obtain the IC spectrum for the isotope from which the transition comes. Thus by gating and projecting the events in each of the  $\gamma$ -peaks that may belong to  $^{61}\text{Ga}$ , hence by also subtracting the background, it is possible to tell what isotope the peak belongs to via the position of the IC spectrum. Figure 3.10 shows the IC spectra for the three nuclei of  $A = 61$  gated on the 124 keV ( $^{61}\text{Zn}$ ), 970 keV ( $^{61}\text{Cu}$ ), and 271 keV ( $^{61}\text{Ga}$ ) peak, respectively.

The procedure is performed for all the six peaks that were found earlier and the result can be seen in Figs. 3.11 and 3.12. It is not always possible to see a peak at the right position in the IC spectrum. However, as long as there is not a peak anywhere else in the spectrum the transition may well belong to  $^{61}\text{Ga}$  and the lack of a peak is only due to the fact that there are too few  $^{61}\text{Ga}$  nuclei produced in the reaction. It is mainly the 1506 keV and the 2137 keV transition that have an undefined IC peak. The other transitions have a more or less well indicated peaks at about the expected position.

### 3.2.4 Recoil- $\gamma\gamma$ Analysis

Six transitions have so far been found as candidates for transitions in  $^{61}\text{Ga}$ . It is now time to test if any of these belong to the same sequence, i.e. whether they are in coincidence with each other. The decay scheme can then be constructed with the excited levels arranged correctly according to which sequence they belong to. To obtain such information a  $\gamma\gamma$  matrix is incremented. It is gated on  $A = 61$  and also restricted to only contain recoils between channels 280-330 on energy loss function #3. The matrix simply shows the different  $\gamma$ -rays from the same event plotted against each other. The two dimensional matrix can be projected down on one of its axes, while it does not matter which one as long as the matrix is symmetric. This spectrum is referred to as the total projection of the  $\gamma\gamma$  matrix.

By gating on a particular peak in this matrix one may obtain a new spectrum in which the  $\gamma$ -rays in coincidence can be investigated. For example, a gate around the 271 keV peak shows a fairly clear peak at 1126 keV indicating that these are in coincidence with each other. Also a small indication of coincidence with the peak

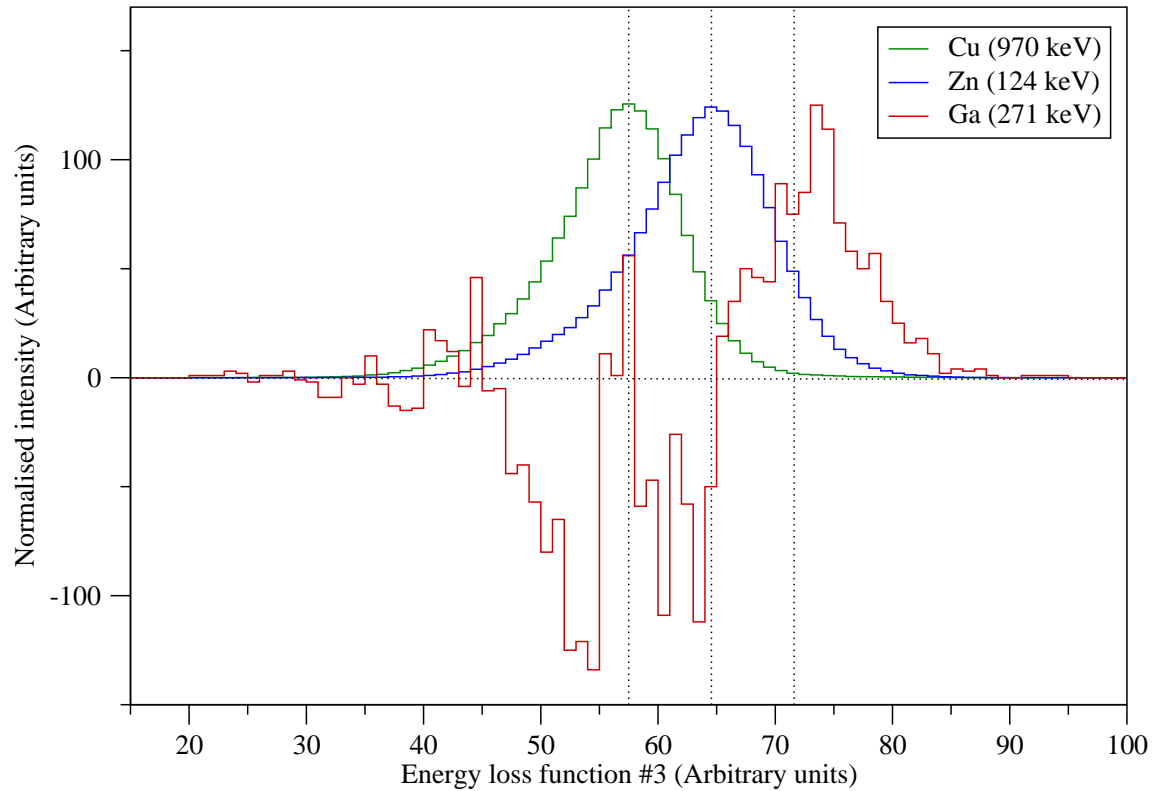


Figure 3.10: IC spectra gated on strong transitions in  $^{61}\text{Cu}$  (green, 970 keV),  $^{61}\text{Zn}$  (blue, 124 keV), and  $^{61}\text{Ga}$  (red, 271 keV). The vertical lines indicates the peak position for  $^{61}\text{Cu}$  and  $^{61}\text{Zn}$ . For  $^{61}\text{Ga}$  the line indicates where the peak should be placed according to estimates in Sec. 3.1.1.

at 1506 keV can be seen in the coincidence spectrum in Fig. 3.13. In the same way one may gate on the 1126 and the 1506 keV peaks to verify a coincidence with the 271 keV  $\gamma$ -ray which is illustrated in Fig. 3.14.

I have here assumed that the transitions at 271, 1126, and 1506 keV belong to the same sequence even though a coincidence between the 1126 and 1506 keV lines would not be established. This assumption is based on mirror symmetry arguments that will be described in more detail in the next section. If this assumption is true one should see coincidence between the 1506 keV and the 1126 keV peak but none is to be seen. This does not necessarily mean that my assumption is wrong but may just indicate that the statistics are too low to give a satisfying coincidence analysis between the transitions.

### 3.2.5 The Decay Scheme

The main contributing force inside a nucleus is the nuclear force, which is thought to be independent of the charge of a particle, i.e., it is possible to view neutrons and protons as two states of the same particle, a nucleon. In order to separate the two states nucleons are assigned a fictitious spin vector called isospin. The isospin has a value of  $1/2$  for both of the nucleons but neutrons have their isospin projection defined in positive direction, spin-up, whereas the proton has its in negative direction, spin-down. Keeping this in mind we are now looking at so called mirror

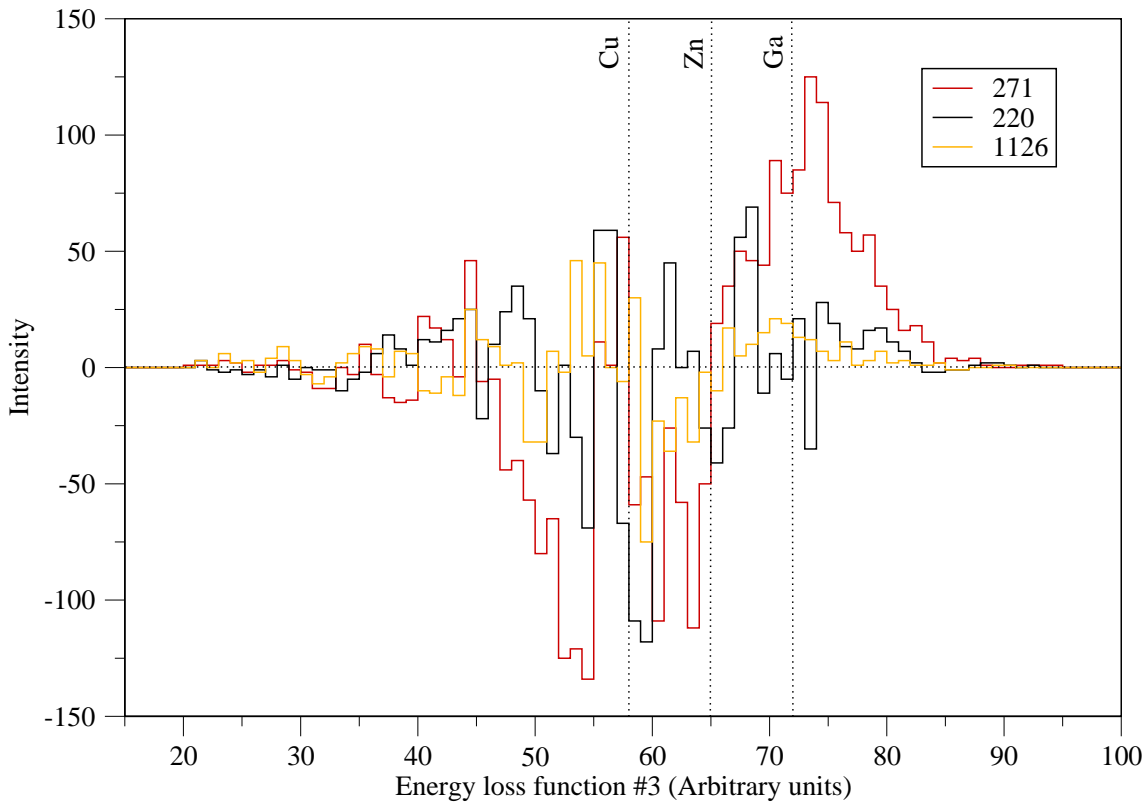


Figure 3.11: IC spectra from the peaks at 220 (black), 271 (red) and 1126 (orange) keV.

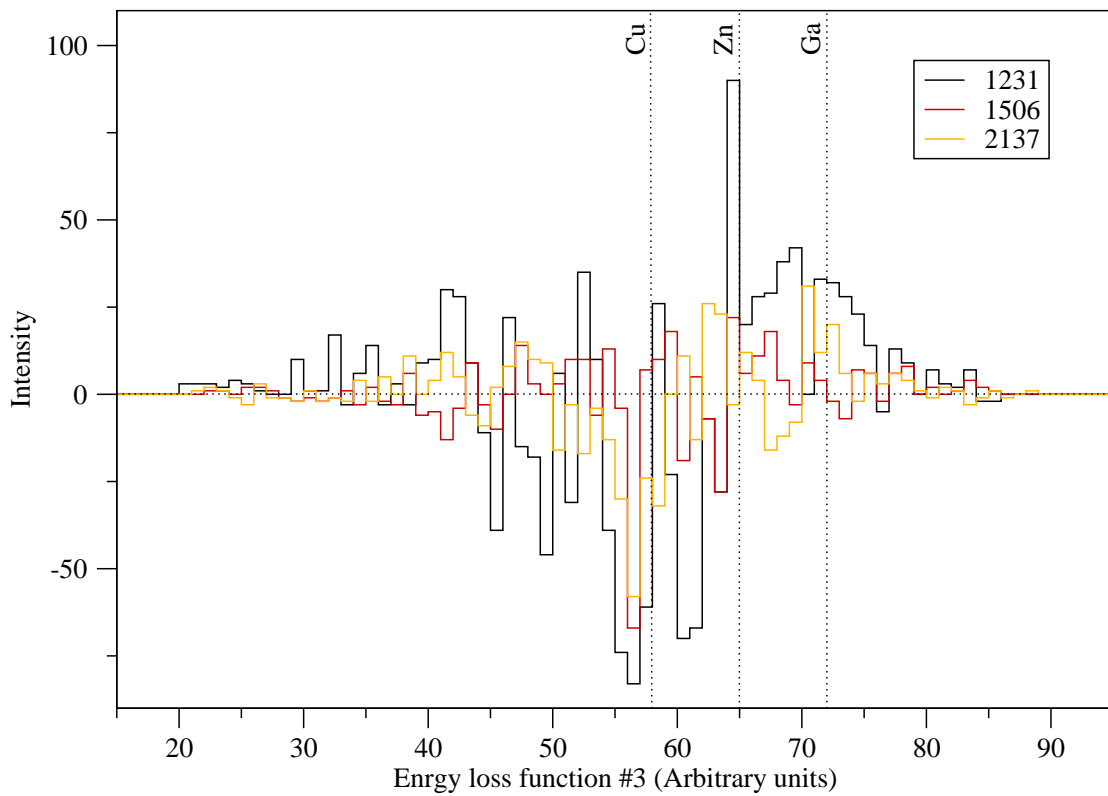
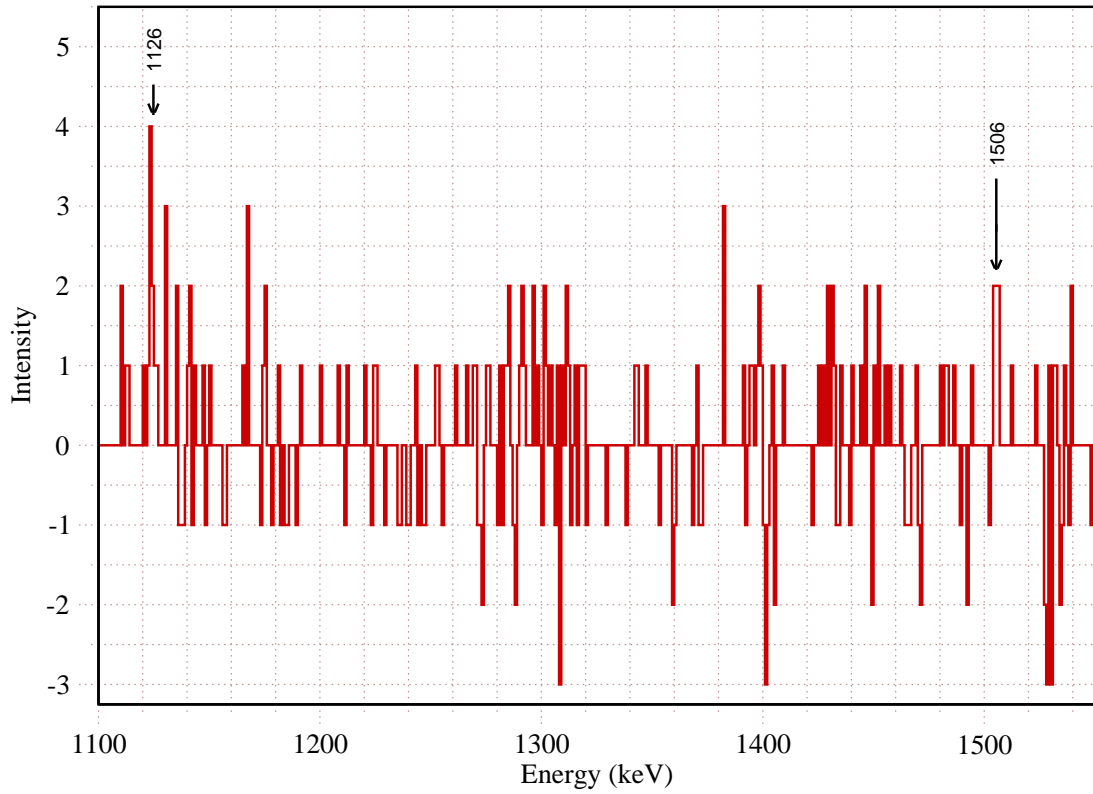
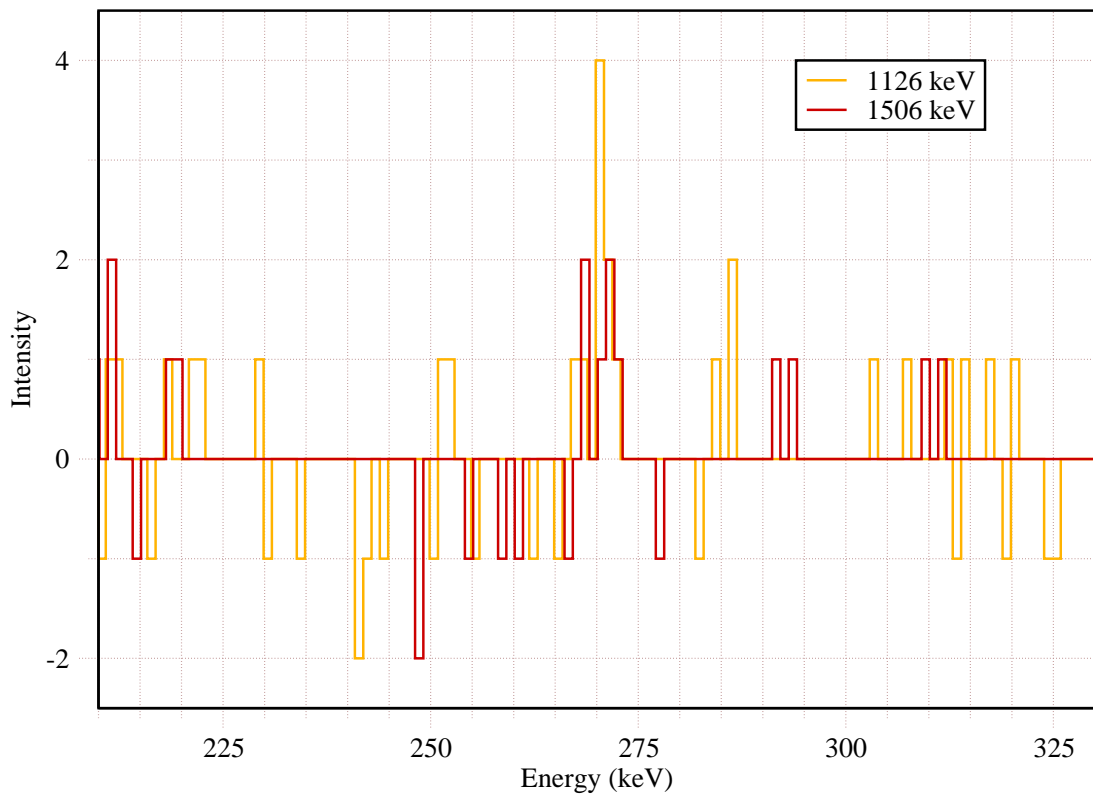


Figure 3.12: IC spectra from the peaks at 1231 (black), 1506 (red) and 2137 (orange) keV.

Figure 3.13: Spectrum in coincidence with the 271 keV peak in  $^{61}\text{Ga}$ .Figure 3.14: The 271 keV  $\gamma$ -ray peak in coincidence with the 1126 keV peak (red) and the 1506 keV peak (orange) in  $^{61}\text{Ga}$ .

nuclei. Mirror nuclei have their proton and neutron numbers interchanged, for example,  ${}^{61}_{30}\text{Zn}_{31}$  and  ${}^{61}_{31}\text{Ga}_{30}$ . Since, as mentioned above, the nuclear force is charge independent the energy levels in the decay schemes of the two nuclei are expected to look similar with equally intense transitions of about the same energies connecting them. It should, however, be mentioned that small differences between the levels in the mirror nuclei, typically 10-100 keV, can be explained via the effect of the symmetry breaking Coulomb force and a part of the nucleon-nucleon interaction that may violate the isospin symmetry.

Transitions in Ga		From	To	Transitions in Zn	
Energy	Intensity			Energy	Intensity
271	$100 \pm 8$	$5/2^-$	$\longrightarrow$ $3/2^-$	124	$100 \pm 3$
1126	$33 \pm 5$	$9/2^-$	$\longrightarrow$ $5/2^-$	1141	$65 \pm 2$
1506	$15 \pm 4$	$13/2^-$	$\longrightarrow$ $9/2^-$	1532	$51 \pm 2$
<hr/>					
220	$12 \pm 3$	$1/2^-$	$\longrightarrow$ $3/2^-$	88	$1.2 \pm 0.1$
1231	$29 \pm 4$	$9/2^-$	$\longrightarrow$ $5/2^-$	1246	$10 \pm 1$
		$11/2^-$	$\longrightarrow$ $7/2^-$	1273	$21 \pm 1$
		$7/2^-$	$\longrightarrow$ $5/2^-$	1279	$3.0 \pm 0.1$
2137	$7.1 \pm 1.7$	$11/2^+$	$\longrightarrow$ $9/2^-$	1979	$3.4 \pm 0.1$
		$13/2^-$	$\longrightarrow$ $9/2^-$	2196	$2.3 \pm 0.1$
		$9/2^+$	$\longrightarrow$ $5/2^-$	2275	$1.2 \pm 0.1$

Table 3.1: Table of transitions identified in  ${}^{61}\text{Ga}$ . The left column lists the transitions that originate from  ${}^{61}\text{Ga}$ . The middle column shows between which states these transitions may occur, and the right column shows the corresponding transitions in the mirror nucleus  ${}^{61}\text{Zn}$ .

Table 3.1 shows the found transitions, which according to the analysis are likely to originate from  ${}^{61}\text{Ga}$  nuclei. The 271, 1126 and 1506 keV transitions are reliable candidates as they are confirmed via the IC spectra and they also are in coincidence with each other. The three remaining transitions are likely to originate from  ${}^{61}\text{Ga}$  but are, however, not completely confirmed. The statistics are too low.

By comparing the energies of the levels involved in the found transitions in  ${}^{61}\text{Ga}$  with the energy levels in the mirror nucleus  ${}^{61}\text{Zn}$ , which has a well known decay scheme, conclusions may be drawn about between which states the transitions take place. Table 3.1 shows the assumptions which are made based on mirror symmetry arguments. The three transitions that are in coincidence are in good agreement with what was expected except for the large energy difference of almost 150 keV between the transition from the  $5/2^-$  state to the  $3/2^-$  ground state in the two

nuclei. This is highly interesting and further discussed in Sec. 4.1. For the three remaining transitions no coincidences have been found which makes it impossible to come to a definite determination of between which states these transitions might appear. The Table shows the possible candidates. A possible decay scheme is shown in Fig. 4.2 but here only the three first transitions from Table 3.1 are included.

### 3.3 Relative Cross-Sections

To calculate the relative cross-sections for the three nuclei of  $A = 61$  involved in this experiment it is sufficient to look at the intensities of transitions to the ground states of the different nuclei.

By looking at the decay scheme of  $^{61}\text{Zn}$  we know that there are five transitions to the  $3/2^-$  ground state at 88, 124, 418, 756, and 996 keV. In the decay scheme of  $^{61}\text{Cu}$  there are also five transitions to the ground state at 970, 1310, 1394, 1733 and 1942 keV. In  $^{61}\text{Ga}$  there are only two transitions found; the 220 and 271 keV which are decaying to the ground state, if the assumptions earlier made are correct.

In theory it would now be sufficient to measure the intensities of these transitions and compare them to get the relative cross-sections but some complications arise due to the fact that the Ge-crystals in CLARION do not detect  $\gamma$ -rays of different energies with the same efficiency. An efficiency calibration has, however, been made earlier, giving us parameters to use in a program, which calculates efficiency corrected intensities. The input of the program should be the intensities of the transitions to the ground state measured in the clean spectra for the  $^{61}\text{Zn}$  and the  $^{61}\text{Cu}$  isotopes and in the  $\gamma$  spectrum obtained by total projection of the recoil- $\gamma$  matrix. The output of the program will then give both the efficiency corrected intensities of the peaks and the intensities expressed as a percentage of the most intense peak that was put into the program, both are obviously given with errors. The problem is that not all of the five ground state transitions in neither  $^{61}\text{Cu}$  nor  $^{61}\text{Zn}$  are clean in the projection of the  $A = 61$  recoil- $\gamma$  matrix, i.e. they may be a mixture of several transitions of the same energy. Using:

$$I(^{61}\text{Cu}) = X * I(\text{strongest/clearest transition}) = I_1 + I_2 + \dots + I_n \quad (3.3)$$

$X$ , can be calculated by adding the intensities from all the  $n$  transitions to the ground state, here denoted  $I_1, \dots, I_n$  from the clean  $^{61}\text{Cu}$  spectrum (c.f. Fig. 3.3). The intensity of the strongest and clearest transition is however measured in the total projection  $\gamma$  spectrum. The same trick can be used for  $^{61}\text{Zn}$  keeping in mind that the strongest and clearest transition in  $^{61}\text{Cu}$  is at 1310 keV and in  $^{61}\text{Zn}$  at 124 keV. When adding the intensities the errors should be calculated too, using the usual error propagation formulae.  $X$  may then be used to calculate the relative cross-sections.

For  $^{61}\text{Ga}$  a different method for calculating the yield is used. Here one may look at the spectrum containing  $^{61}\text{Zn}$  and  $^{61}\text{Ga}$  to find the intensities for the  $^{61}\text{Ga}$  transitions. These intensities are efficiency corrected in the program mentioned above. However, the spectrum is obtained via the gate in Fig. 3.2 and hence it does not include all the  $^{61}\text{Ga}$  recoils (c.f. Fig. 3.10 where the gate would be placed between

the corresponding values 75-85 of energy loss function #3, i.e. not even half of the  $^{61}\text{Ga}$  recoils are included in the spectrum). By comparing the area of the total IC spectrum with the area of the part of the spectrum included in the gate it is found that only  $(40\pm 5)\%$  of the  $^{61}\text{Ga}$  peak are included in the spectrum. When performing the necessary calculations including the errors the following relative intensities are obtained.

$$\begin{aligned}I_{rel}(\text{Cu}) &= 190 \pm 6 \\I_{rel}(\text{Zn}) &= 77 \pm 6 \\I_{rel}(\text{Ga}) &= 0.32 \pm 0.04\end{aligned}$$

This means that for every 600  $^{61}\text{Cu}$  nuclei being produced in the fusion evaporation reaction 240  $^{61}\text{Zn}$  nuclei will be produced and only one  $^{61}\text{Ga}$  nucleus.

## Chapter 4

# Comparing Theory and Experiment

The energy, spin, and parity of the excited levels in a nucleus as well as their sequence and decay patterns can be calculated with the shell-model. A shell-model can be based, for example, on an average potential such as the Woods-Saxon potential which is given by:

$$V(r) = \frac{-V_0}{1 + e^{\frac{r-R}{a}}} \quad (4.1)$$

$R$  is the mean radius of the nucleus given by  $R = 1.25A^{1/3}$ ,  $a$  is the skin diffuseness ( $a=0.524$  fm),  $r$  is the distance from the centre of the nucleus, and  $V_0$  is the depth of the potential well (in the order of 50 MeV).

An average potential, which is generated by all the nucleons is, however, not sufficient to describe the nuclear structure. It has to be combined with a spin-orbit interaction, which will make the shells split into subshells, giving rise to the magic numbers that have been experimentally confirmed at several occasions [7]. Magic numbers correspond to the number of nucleons that represent filled major shells and have been found at  $Z$ ,  $N = 2, 8, 20, 28, 50, 82$ , and  $N = 126$ . In the same way as atomic physics ascribes the properties of the atom to the valence electrons one may in nuclear physics ascribe the properties of the nucleus to the nucleons in the last unfilled subshell.

The excited states of  $^{61}\text{Ga}$  involved in the transitions listed in Table 3.1 may arise through the placement of nucleons in the relevant subshells as illustrated in Fig. 4.1. Two valence nucleons tend to couple their spin together, i.e. in spin zero pairs. These nucleons will then not contribute to the total spin of the state. It is, however, possible to break nucleon pairs and re-couple their spins. Looking at Fig. 4.1 one should keep in mind that no state is “pure” but they all consists of a mixture of wave functions from different configurations that may result in the same quantum numbers. For any state there is, however, normally one configuration that is dominating. Some states are more mixed than others and for a given state it is possible to calculate the wave function contribution from different configurations with a contemporary shell-model code **Antoine**, which will be mentioned further in the next section.

Looking at the decay scheme of  $^{61}\text{Zn}$ , Fig. 4.2, keeping in mind that this is the

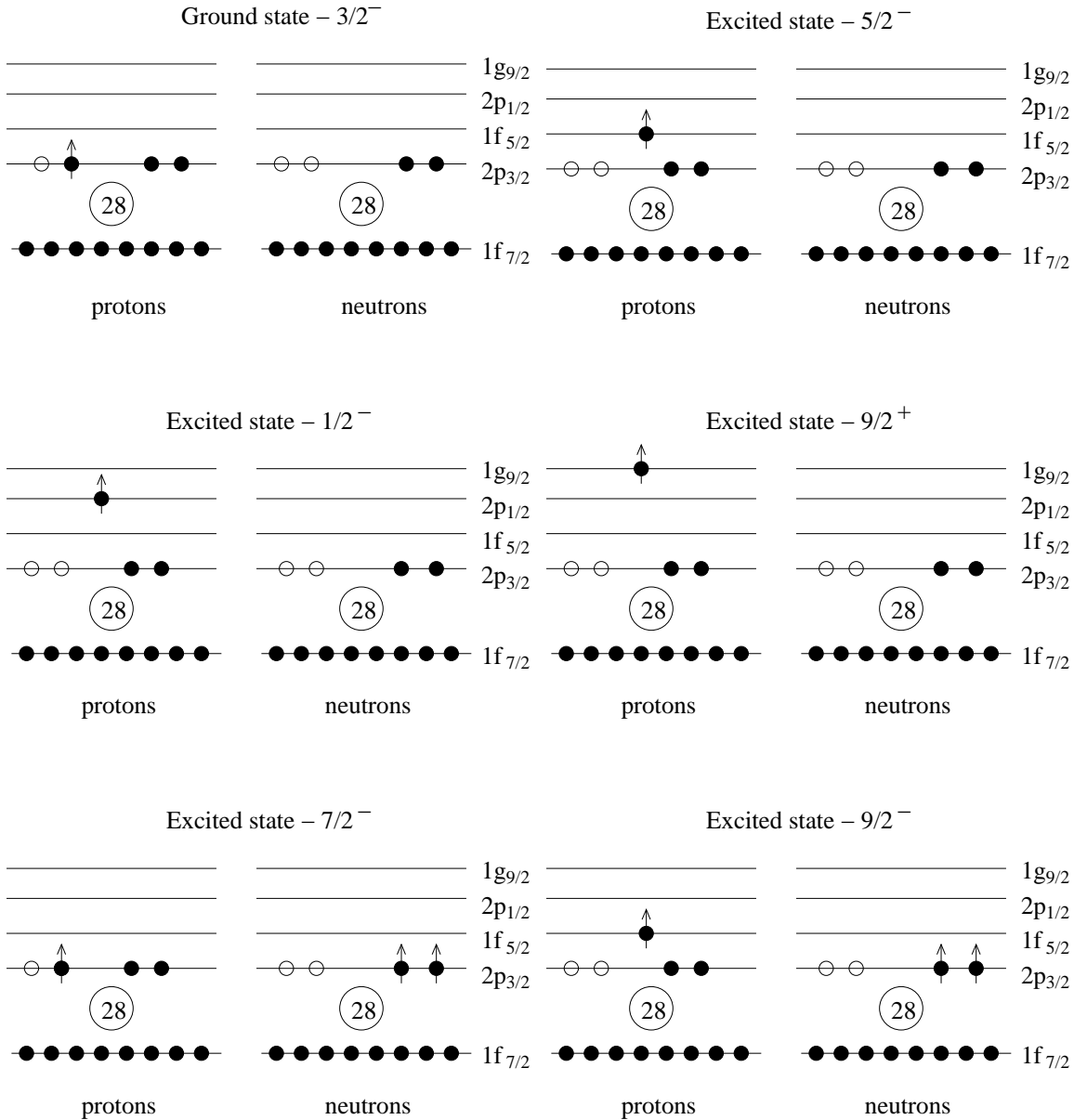


Figure 4.1: An illustration of possible configurations for  $^{61}\text{Ga}$ . Filled (open) circles indicate particles (holes), encircled digits indicated the magic numbers. The figure only includes the excited levels that might be involved in the transitions found in the analysis of this experiment. The  $11/2^-$  and  $13/2^-$  states have not been included as they are mixed to a larger extent than the states illustrated here. See text for details. The first four states  $3/2^-$ ,  $5/2^-$ ,  $1/2^-$ , and  $9/2^+$  can be created by moving the odd single proton between the available subshells. The  $7/2^-$  and  $9/2^-$  states require the breaking and alignment of a pair of neutrons (or protons).

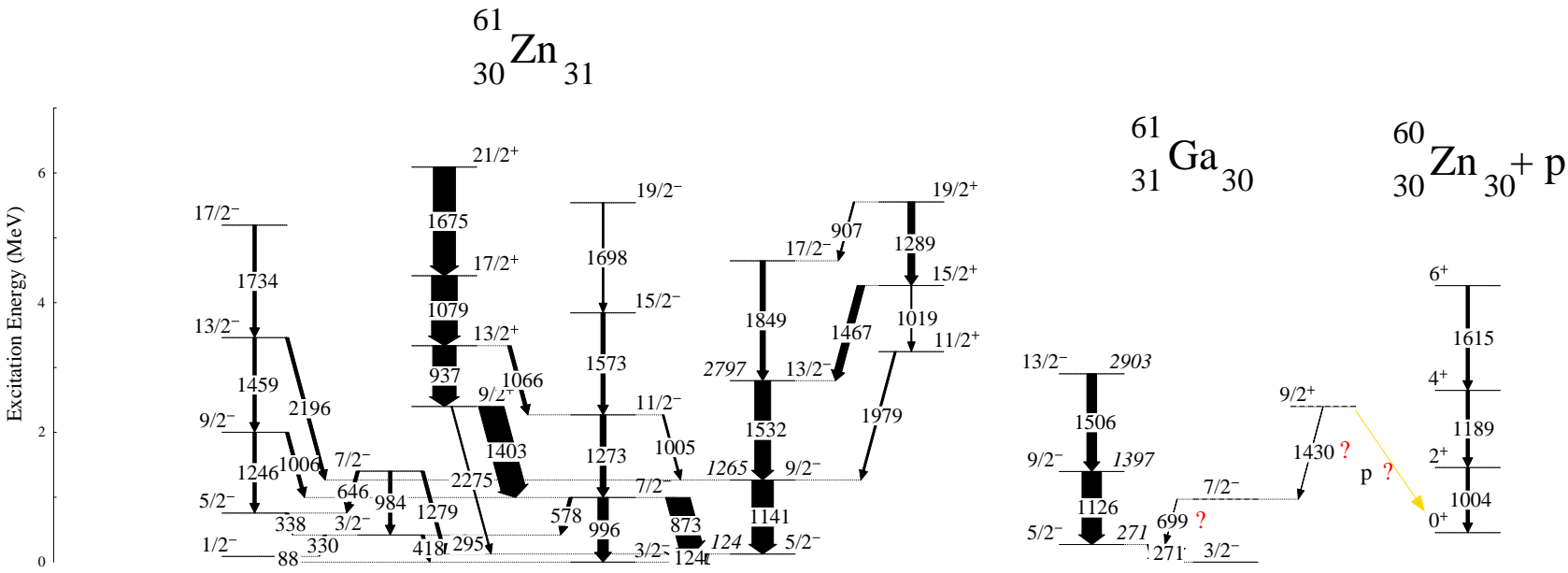


Figure 4.2: A possible decay scheme of  ${}^{61}\text{Ga}$  and the well known levels in  ${}^{61}\text{Zn}$  and  ${}^{60}\text{Zn}$ . A possible proton decay between the (hitherto non-observed)  $9/2^+$  state of  ${}^{61}\text{Ga}$  and the  $0^+$  ground state in  ${}^{60}\text{Zn}$  is indicated with an arrow. Note that the 699 keV and the 1430 keV transitions in  ${}^{61}\text{Ga}$  have not been found.

mirror nucleus of  $^{61}\text{Ga}$  it is surprising to see that strong transitions such as those at 873, 996, 1403 and maybe even 937 keV have not been found in the  $^{61}\text{Ga}$  spectrum. (High intensity transitions at higher spin are not very probable as the beam energy used in this experiment is too low to populate high-spin states.) One explanation to why these transitions have not been found may be that  $^{61}\text{Ga}$  might undergo prompt proton decay, which would not be seen here at all. Prompt proton decay [8] competes with  $\gamma$ -radiation in nuclei close to the proton drip line and by emitting a proton the  $^{61}\text{Ga}$  nucleus may decay into  $^{60}\text{Zn}$ . Looking at the excited states in the two nuclei one may see that there is a striking resemblance between the two. The  $4^+$  state of  $^{60}\text{Zn}$  decays via a 1189 keV  $\gamma$ -ray into the  $2^+$  state and the  $2^+$  decays with a 1004 keV  $\gamma$ -ray into the ground state. In the same way the  $17/2^+$  state in  $^{61}\text{Ga}$  decays via a 1079 keV  $\gamma$ -ray into the  $13/2^+$  state which in turn decays via a 937 keV  $\gamma$ -ray into the  $9/2^+$  state. It is easy to make the connection that since the proton is very loosely bound (its binding energy is only about 190 keV [9]) it may be emitted; transporting the  $^{61}\text{Ga}$ -nucleus into an energy level in  $^{60}\text{Zn}$ . Looking at the probabilities for the proton to be emitted with different angular momenta and with different energies it turns out that the  $9/2^+$  state in  $^{61}\text{Ga}$  is most likely to decay into the ground state of  $^{60}\text{Zn}$ , similarly it is likely for the  $13/2^+$  state to decay into the  $2^+$  state and so on, populating all the levels in the sequence of  $^{60}\text{Zn}$  shown in Fig. 4.2.

## 4.1 Mirror Energy Difference

It has already been mentioned that the corresponding energy levels in two mirror nuclei are expected to be placed of about the same excitation energies. This is, however, not exactly the case. A way to compare these energies is to use a Mirror Energy Difference (MED) plot. The  $x$ -axis will here represent the spin quantum number  $J$  and the  $y$ -axis the energy difference of the levels, calculated by subtracting the energy of a level in the mirror nucleus with the larger proton number from the energy of the same level in the nucleus with the larger neutron number. Figure 4.3 shows the results for  $^{61}\text{Ga}$  and  $^{61}\text{Zn}$ . The values are only plotted for the well determined levels. Theoretical values are calculated for yrast<sup>1</sup> states with the program package *Antoine* in a KB3G interaction [10, 11] with three particle excitations from  $1f_{7/2}$  to the upper fp shell allowed.

Two calculations have been performed: the black plot, referred to as #1, is calculated with 1.8 MeV energy difference for neutrons and 2.0 MeV for protons between the  $1f_{7/2}$  and the  $2p_{3/2}$  orbitals. The blue plot is only calculated as a reference and the same energy difference, 2.0 MeV, between the two orbitals is used. No distinction is in this case made between protons and neutrons. The difference in separation energy used in the first calculation is, however, experimentally confirmed and may be explained with the electromagnetic spin-orbit interaction [12]. According to this interaction the energy difference between the two orbitals in neutrons and protons differ due to quantum mechanical reasons and the decay scheme will hence differ between the mirror nuclei.

---

<sup>1</sup>The state which has the lowest possible energy for a given spin.

It is easy to see in Fig. 4.3 that the experimental results strongly indicate that there is in fact an electromagnetic spin-orbit contribution to the MED, since they agree best with calculation #1. Figure 4.3 illustrates the big impact this interaction has on the energies of the nuclear levels.

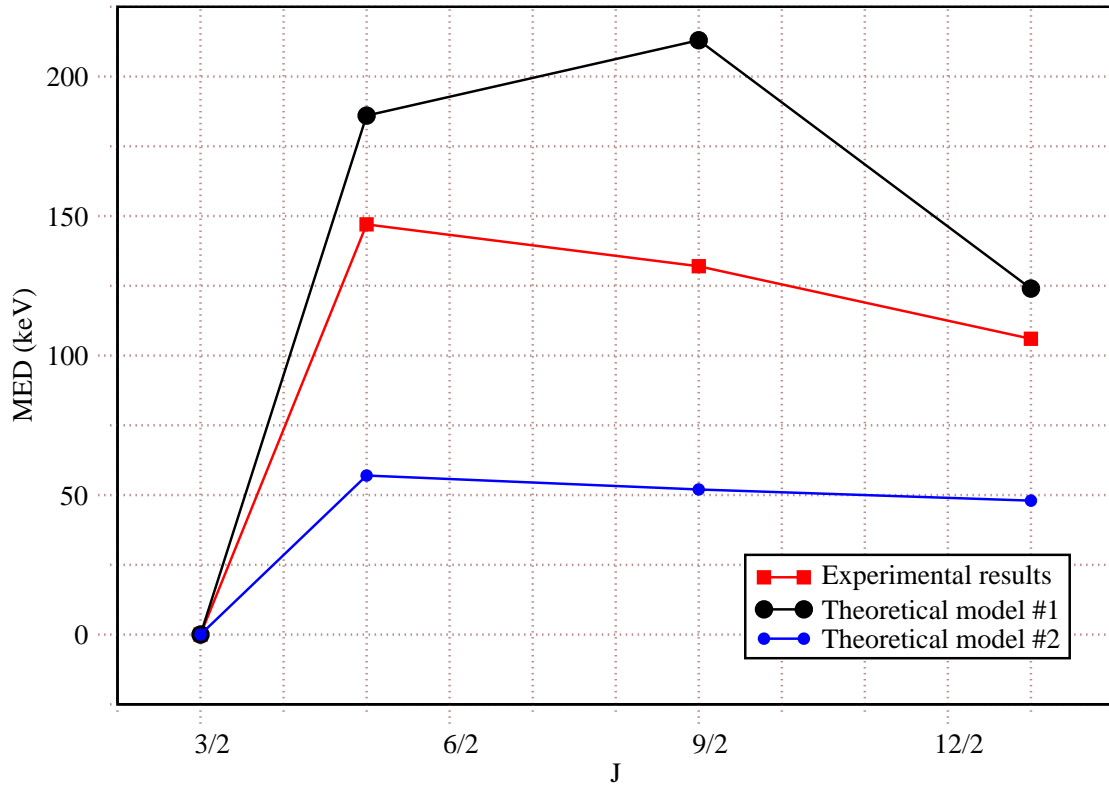


Figure 4.3: The mirror energy difference plot for  $^{61}\text{Ga}$  and  $^{61}\text{Zn}$ . The red plot shows the experimental energy difference between corresponding energy levels. Only the  $3/2^-$ ,  $5/2^-$ ,  $9/2^-$ , and  $13/2^-$  states are included. The black plot shows the mirror energy difference according to theoretical calculations performed according to model #1 and the blue are calculated according to model #2. See text for details.



# Chapter 5

## Conclusion and Outlook

Six possible transitions from  $^{61}\text{Ga}$  have been found. Three of them, placed at 271, 1126, and 1506 keV, are confirmed via coincidences and IC spectra. This makes it possible to determine the spin and parity of the excited states via mirror symmetry arguments. The remaining three transitions, placed at 220, 1231, and 2137 keV, need additional statistics in order to make a complete analysis and determination of the spin and parity of the states.

The large energy difference between the  $5/2^-$  states and the  $3/2^-$  ground states in the mirror nuclei  $^{61}\text{Ga}$  and  $^{61}\text{Zn}$  may be explained by the electromagnetic spin-orbit interaction. Similar energy differences (almost 300 keV) have been observed earlier in mirror nuclei, for example, in  $^{35}\text{Ar}$  and  $^{35}\text{Cl}$  [12].

As mentioned in the introduction we experienced complications with the ion source during the experiment. This resulted in some 50 % loss in beam time which, of course, has a big impact on the number of detected recoils. This gives a lack in statistics that would be useful in order to confirm the transitions in  $^{61}\text{Ga}$  via the IC spectra, which will become a lot clearer if additional beam time would be received. Extra beam time would also make it possible to confirm the coincidences via the recoil- $\gamma\gamma$  matrix and would help in the placement of the 1231 keV and the 2137 keV transitions as coincidences with  $\gamma$ -rays originating from lower transitions would allow a determination about between which levels the transitions take place. Therefore, in order to complete the analysis, 3-4 days of compensational beam time are requested from the Holifield Radioactive Ion Beam Facility at the Oak Ridge National Laboratory.

As mentioned in Sec. 3.2.5 the  $^{61}\text{Ga}$  nucleus may undergo prompt proton decay due to the fact that the unpaired valence proton is very loosely bound to the nucleus. This will obviously have to be investigated further before any final conclusions about this possible decay may be drawn. During the spring of 2004 an experiment is planned at Argonne, Illinois. The experiment is unique in its kind as it will, for the first time, make it possible to perform particle spectroscopy in coincidence with recoils and  $\gamma$ -radiation. The experiment will be run at 136 MeV beam energy with a  $^{28}\text{Si}$  target and  $^{36}\text{Ar}$  beam, i.e. it will again be possible to open a reaction channel to form  $^{61}\text{Ga}$  nuclei, this time even high spin states may be produced. The p2n reaction channel has its maximum placed at around 120 MeV (c.f. Fig. 1.3) but the experiment has been granted a long run time and it may then still be possible to produce and detect enough  $^{61}\text{Ga}$  nuclei to continue, and extend, the analysis.



# Acknowledgements

I would like to thank Prof. Claes Fahlander for giving me the opportunity to join the Lund research group of nuclear structure and for his kind advice and interest.

I also would like to thank my supervisor Dirk Rudolph, without whom this project would not have been possible to complete. I am grateful for the hours we have spent together in front of the computer, for your patients with me and my questions and for always supporting me throughout this project.

Also thanks to Emma with whom I have shared office, thoughts and laughs these last six months. May you always think that science is awesome! I do hope we will remain co-workers in the future as well!

Thanks to the rest of the people working in and together with the Nuclear Structure Group in Lund that have showed interest in my work during the semester. Especially thanks to Rickard du Rietz and Jörgen Ekman for their help and patience and to Gavin Hammond at Keele University, UK for helping out during the experiment.

My gratitude also goes to all the people working at the Oak Ridge National Laboratory for making my first visit to the States pleasant and for helping out when nothing seemed to work. Especially thanks to Carl Gross and David Radford for their expertise.

Last but not least I want to thank My, BellBell and Aisa for their love and support, I hope that reading this report will make you realise that Physics is fun! :)



# Bibliography

- [1] E.K. Johansson, Master thesis, Lund University, LUNFD6/(NFFR-5023)1-47/(2004).
- [2] [www.phy.ornl.gov/hribf/research/equipment/clarion/](http://www.phy.ornl.gov/hribf/research/equipment/clarion/)
- [3] G.D. Alton, J.R. Beene, J. Phys. G: Nucl. Part. Phys. **24**, 1347-1359 (1998).
- [4] [www.phy.ornl.gov/hribf/research/gallery/ic\\_land.html](http://www.phy.ornl.gov/hribf/research/gallery/ic_land.html)
- [5] C.J. Gross *et al.*, Nucl. Instrum. & Meth. in Phys. Res. A **450**, 12-29 (2000).
- [6] G.F. Knoll, "Radiation and Measurement", 2nd edition, John Wiley & Sons, New York (1989).
- [7] K.S. Krane, "Introductory Nuclear Physics", John Wiley & Sons, New York (1988).
- [8] D. Rudolph *et al.*, Phys. Rev. Lett. **80**, 3018, (1998).
- [9] L. Weissman *et al.*, Phys. Rev. C **65**, 044321, (2002).
- [10] E. Caurier, shell model code ANTOINE, IRES, Strasbourg (1989-2002).
- [11] E. Caurier, F. Nowacki, Acta Phys. Pol. **30**, 705 (1999).
- [12] J. Ekman *et al.*, "Unusual Isospin-Breaking and Isospin-Mixing Effects in the  $A = 35$  Mirror nuclei", submitted to Phys. Rev. Lett.